Immunomodulatory properties of an arabinan polysaccharide extracted from Sida cordifolia: isolation, characterization and in vitro mechanism of action

Cheng, F., Pan, X., Notaro, A., Iovine, A., Molinaro, A., De Castro, C., & Green, B. D. (2025). Immunomodulatory properties of an arabinan polysaccharide extracted from Sida cordifolia: isolation, characterization and in vitro mechanism of action. *Carbohydrate Polymers*, *363*, Article 123724. https://doi.org/10.1016/j.carbpol.2025.123724

Published in:
Carbohydrate Polymers

Document Version:
Publisher's PDF, also known as Version of record

Carbohydrate Polymers 363 (2025) 123724

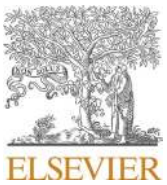

Contents lists available at ScienceDirect

Carbohydrate Polymers

journal homepage: www.elsevier.com/locate/carbpol

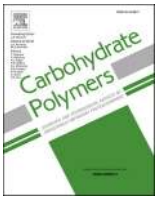

Immunomodulatory properties of an arabinan polysaccharide extracted from *Sida cordifolia*: isolation, characterization and *in vitro* mechanism of action

Fang Cheng [a], Xiaobei Pan [a], Anna Notaro [b], Andrea Iovine [b], Antonio Molinaro [b], Cristina De Castro [b], Brian D. Green [a,*]

[a] *School of Biological Sciences, Institute for Global Food Security, Queen's University Belfast, Belfast, UK*
[b] *Department of Chemical Sciences, University of Napoli Federico II, Italy*

ARTICLE INFO

Keywords:
Sida cordifolia
Malvaceae
Arabinan
Metabolic response
Mechanism-of-action
Immunomodulator

ABSTRACT

An arabinan polysaccharide of low molecular weight (SC-S50, 3.2 KDa) and a structurally-related high molecular weight arabinan (SC-P50, 66 KDa) were isolated from *Sida cordifolia* root. NMR spectroscopy revealed the two polysaccharides were structurally similar consisting of three motifs, the main one being an α-L-arabinofuranose disaccharide (A-(1 → 5)-D) in the linear backbone; the A unit is further substituted at *O*-2 and *O*-3 positions by α-L-arabinofuranose. The two minority motifs also consist of α-1 → 5 linked L-arabinofuranose disaccharide, but in contrast, the A unit is replaced by the E or F unit, which is substituted by α-L-arabinofuranose only at the *O*-2 or *O*-3 position. SC-S50 did not activate macrophages cells *in vitro,* but in contrast, SC-P50 potently stimulated nitric oxide production in RAW264.7 macrophages (EC50: 7.92 μg/mL). SC-P50 significantly increased pinocytosis (phagocytosis), cell proliferation and cytokine secretion (IL-2, IL-6, TNF-α, IL-8), with minimal cytotoxicity. SC-P50 was then screened in 12 human primary cell-systems simulating various human tissue and disease characteristics. In 10 of these cell systems SC-P50 increased the production of IL-8. Mechanism-of-action studies unpicked the receptors, intracellular signalling and metabolic responses underlying SC-P50's immunomodulatory actions. SC-P50 is a novel immunomodulatory plant-derived polysaccharide which should be evaluated for its ability to prevent/treat infection.

1. Introduction

Recent years have seen an increased focus on the discovery of natural immunomodulatory compounds (Khairy et al., 2023; Pillai & Antony, 2024; Zebeaman et al., 2023). Also referred to as biological response modifiers, these compounds can interact with the immune system to up- or down-regulate specific aspects of a host's response. Plant compounds with such biological activities include alkaloids, flavonoids, terpenoids, polyphenols, polysaccharides, lignans, essential oils, saponins, tannins and phytosterols (Costa et al., 2016; Dabravolski et al., 2023; Guo et al., 2024; Huyke et al., 2007; Jin et al., 2014; Klos & Chlubek, 2022; Michalak, 2022; Peng et al., 2019; Rajasekaran et al., 2021; Samtiya et al., 2021; Shen et al., 2024; Xue et al., 2019).

Immunomodulatory plant polysaccharides are particularly interesting, inducing immune responses during infection and influencing innate and cell-mediated immunity by interacting with various immune cells, such as T-cells, natural killer cells, and macrophages (Huang et al., 2022; Surayot & You, 2017; Tabarsa et al., 2020). Appropriate modulation of the immune response by these polymers has been shown to improve a host's ability to fight various infections (Murphy et al., 2023; Panggabean et al., 2022; Sindhu et al., 2021; Song et al., 2020). Polysaccharides can also be used to improve current treatments, particularly antimicrobial therapies which are becoming less effective due to antimicrobial resistance (AMR) (Ayrapetyan et al., 2021; Balducci et al., 2023; Lai et al., 2024). Thus far, very few polysaccharide immunomodulators have been examined in detail, and structure-activity studies are typically lacking.

A common approach in the discovery of novel immunomodulatory compounds involves testing their ability to activate nitric oxide (NO) production in macrophages (Iqbal et al., 2022). It also can be useful to determine to what extent they promote an 'M1' or 'M2' state. Macrophages typically exist in a baseline 'M0' state and can be polarised to M1

* Corresponding author.
E-mail address: b.green@qub.ac.uk (B.D. Green).

https://doi.org/10.1016/j.carbpol.2025.123724
Received 10 March 2025; Received in revised form 16 April 2025; Accepted 7 May 2025
Available online 9 May 2025

macrophages (pro-inflammatory) by treating with lipopolysaccharide (LPS), which activates Toll-like receptors (TLRs) (Chen et al., 2023). M0 can also be polarised to an M2 (anti-inflammatory) state by treating with interleukins such as IL-4 or IL-13, acting *via* their respective receptors (Laskin, 2009). The transition to M1 or M2 can be determined either by identifying which receptors/intracellular activates. For example, TLR-4 and NF-κB are important signalling components of M1 with STAT/SMAD signalling involved in M2 (Biswas & Mantovani, 2012). The transition from M0 to M1 or M2 can also be monitored by changes in cellular metabolism. M1 macrophages rely heavily on glycolysis (Jha et al., 2015) whereas M2 macrophages rely on beta-oxidation and glutaminolysis (Vats et al., 2006).

The present investigation undertook a detailed characterization of the immunomodulatory glycans present in a perennial subshrub named *Sida Cordifolia,* a member of *Malvaceae* family. *S. cordifolia* is used widely in Indian, Chinese, African, Brazilian and American traditional medicines to address conditions such as oral mucositis, bronchial asthma and nasal blockage (Dinda et al., 2015; Franco et al., 2005; Franzotti et al., 2000; Rodrigues & de Oliveira, 2020). Our research group reported that an aqueous extract of *S. cordifolia* root powder possessed potent and broad-ranging immunomodulatory activities, including the ability to stimulate lymphocyte proliferation, augment IgG production, enhance macrophages phagocytosis, and upregulate the expression of several cytokines in RAW 264.7 cells (Iqbal et al., 2022). The extract appeared to contain a complex mixture of different polysaccharides, and it was possible to enhance their activity by the further enrichment of the polysaccharide fraction. The aim of the present study was to isolate individual immunomodulatory polysaccharides, to resolve their precise structure, then to determine the cellular mechanism of action of any purified polysaccharides.

Ultimately one low molecular weight, and one larger structurally-related arabinan, were isolated, purified and structurally elucidated. The low molecular weight arabinan (SC-S50) was inactive, but the higher molecular weight arabinan (SC-P50) was highly potent and its biological activities were characterized in detail. The purified *S. cordifolia* arabinan (SCA), was structurally characterized by profiling of its monosaccharide composition, partially methylated alditol acetates (PMAA) and nuclear magnetic resonance (NMR). Subsequently, the bioactivities of SC-P50 were confirmed in RAW 264.7 cells by measurement of nitrite oxide (NO) production, pinocytosis, proliferation and cytotoxicity. Additionally, this arabinan's ability to stimulate the secretion of several cytokines were evaluated, and this involved the measurement of IFN-γ, IL-2, IL-1β, IL-4, IL-6, IL-12, TNF-α and IL-10 secretion from RAW 264.7 cells. Moreover, SC-P50 was characterized using the BioMAP Diversity PLUS panel of 12 primary human cell-based systems which have been engineered to simulate intricate human tissue and disease characteristics related to the vascular system, skin, lungs, and inflammatory tissues. Precise assessments of biomarker activities within this diverse array, combined with a comparative evaluation of the biological effects of established bioactive substances present in a reference database, serve as a means of forecasting the safety, effectiveness and functionality of SC-P50. SC-P50 increased the production of IL-8 in 10 human primary cell-based systems. This prompted a series of studies in RAW 264.7 cells transfected with an IL-8 reporter gene (IL-8 LucRep-RAW 264.7 cells) which unpicked the underlying mechanisms for SC-P50 induction of NO production, IL-8 expression and IL-8 secretion. Finally, LC-MS/MS metabolomic profiling was conducted to assess the various metabolic responses of RAW 264.7 cells to SC-P50. The findings presented herein contribute valuable insights into the immunomodulatory potential of a novel plant-derived polysaccharide with future therapeutic potential.

2. Materials and methods

2.1. Chemicals and reagents

S. cordifolia root powder was purchased from Pukka Herbs® (Keynsham, UK). Chemicals and reagents used were of the highest analytical grade available and are listed in Supplementary Method S1.

2.2. Extraction of S. cordifolia

S. cordifolia root powder (2 g) (Fig. 1) was soaked in 95 % ethanol (15 mL) at room temperature (R.T.) overnight (o.n.) under stirring and then centrifuged at 4 °C for 30 mins at 6500 rpm. The supernatant was discarded while the precipitate was collected in a laboratory bottle with a screw cap, suspended in ultra-pure water (15 mL) and stirred at 100 °C for 1 h in an oil bath on a hotplate stirrer (Stuart, Merck, UK) coupled to a temperature controller (Stuart, VWR, UK). The suspension was centrifuged at 4 °C for 30 mins at 6000 rpm, and the supernatant was collected. This step was repeated five times, and the different supernatants were pooled together and reduced to approximately one-fifth volume by a rotavapor (Büchi, rotavapor R-200, Merck, UK). This solution was digested with (1 mg) α-amylase and (250 μL, ~ 250 NPUN) pullulanase for 7 h, followed by digestion with (1 mg) Proteinase K (1 mg) overnight. After the enzymatic digestion, the solution was dialyzed against ultrapure water (molecular weight cut-off of 3.5 kDa), with water changes every 2–3 h for a total of three changes. The solution inside the dialysis tube presented some precipitate that was removed by centrifugation (30 mins at 6000 rpm) and 95 % ethanol was added to the

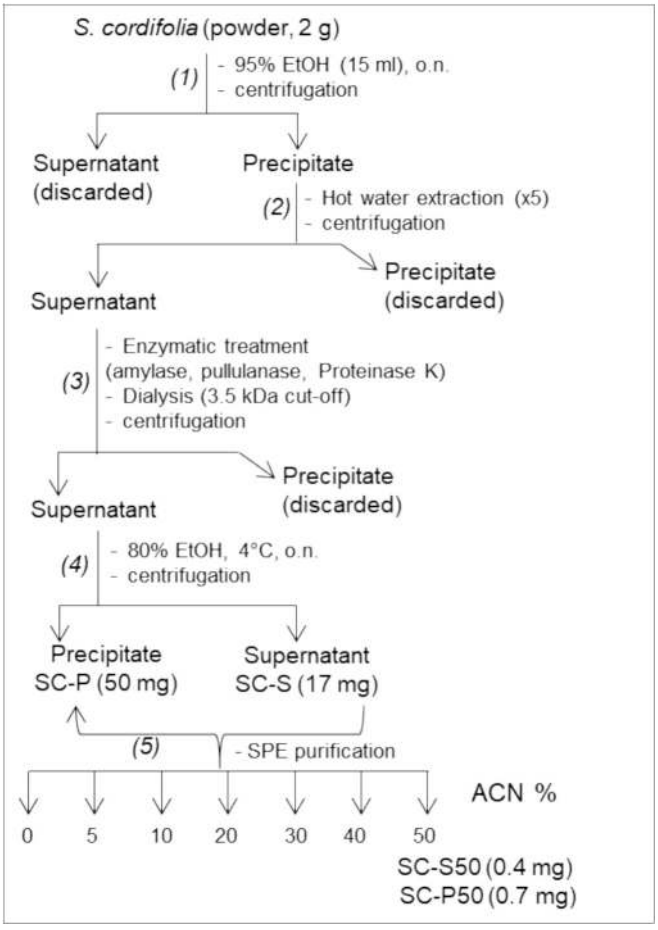

Fig. 1. Purification scheme used to isolate the arabinan (SC-S50 and SC-P50) from *S. cordifolia* root powder.

clear supernatant to reach 80 % final concentration, the solution was left at 4 °C overnight and the resulting precipitate was separated by the supernatant by centrifugation (30 mins at 6000 rpm).

The precipitate (SC-P) was solved in water and freeze-dried to yield 50 mg, while the supernatant (SC-S) was dried with dried with a rotary evaporator, and the resulting solid was solved in water and freeze-dried to yield to 17 mg. Both SC-P and SC-S were checked by proton NMR and chemical analysis.

2.3. Solid phase extraction (SPE) purification of SC-S

The crude product was dissolved in water (3 mL) and purified by using a Hypercarb™ SPE Cartridge. Prior use, the cartridge was activated by washing with the following solutions: 1 M NaOH (12 mL), water (24 mL), 30 % acetic acid (12 mL), water (24 mL), 50 % ACN (12 mL), 5 % ACN (24 mL) and water (30 mL). The sample was dissolved in water and the separation was performed, by varying in a stepwise manner, the ACN content of the eluent, so that the fractions (15 mL each) collected were 0, 5, 10, 20, 30, 40 and 50 % in the organic solvent, each labelled by adding the ACN % as suffix to the initial name (*e.g.* SC-S0 indicated 0 % ACN content). Finally, the cartridge was regenerated with ACN 100 % and TFA 0.1 M. ACN was removed from all fractions using a rotary evaporator, the resulting water solutions were freeze-dried and the material recovered was checked by proton NMR.

2.4. Structural characterization of SCA

2.4.1. Molecular weight determination of SCA

The molecular weight of the samples was determined by SEC-HPLC (TSK gel G5000 PW_{XL}, 30 cm × 7.8 mm I.D.). The sample (30 μL, 1 mg/mL solution) was injected on the TSK column and eluted with 50 mM ammonium bicarbonate (flow 0.8 mL/min). The eluate was monitored with a refractive index detector, using a HPLC Agilent 1100 system. The column was calibrated with dextrans of known molecular weight (5, 50, 150, 410, and 610 kDa), the data were fitted by linear regression and the molecular weight of sample was evaluated accordingly.

2.4.2. Monosaccharide analysis

The monosaccharide composition was established by analysing the corresponding acetylated *O*-methyl glycoside derivatives. SCA (~ 0.2 mg) was treated with HCl/MeOH (1.25 M, 80 °C, 16 h). The solvent was removed under air flow and the methyl glycosides acetylated with acetic anhydride (50 μL) in pyridine (100 μL) at 80 °C for 30 min (De Castro et al., 2010), prior to GLC-MS analysis (See Supplementary Methods S2).

2.4.3. NMR spectroscopy

NMR spectra were recorded in deuterated water (D_2O) at 298 K by using a Bruker 600 MHz spectrometer equipped with a reverse cryoprobe with gradients along the z-axis. All spectra were calibrated with acetone as the internal standard (^{1}H 2.225 ppm; ^{13}C 31.45 ppm). The 2D set of NMR spectra comprised Correlation Spectroscopy (COSY), total correlation spectroscopy (TOCSY), and Nuclear Overhauser enhancement spectroscopy (NOESY) experiments, all performed by using data sets (t1 × t2) of 2048 × 512 points, TOCSY and NOESY mixing time was set to 100 and 200 ms, respectively. Heteronuclear single-quantum coherence (HSQC), and heteronuclear multiple-bond correlation (HMBC) experiments were performed using sets of 2048 × 512 points. HMBC was optimized for 6–15 Hz coupling constants, while the mixing time of the HSQC-TOCSY was set to 80 ms. Spectra were transformed and analysed with Topspin 3.6 and/or or 4.0 version.

2.5. In vitro immunomodulation properties of SCA

2.5.1. NO production

RAW 264.7 cells were cultured as described in Supplementary Method S3. The NO production was determined using the Griess assay. Briefly, cells were seeded at a density of 1×10^5 cells per well into a 96-well microplate. Cells were incubated for 24 h (37 °C; 5 % CO_2). Cells were then stimulated with serially diluted test agents (3.125–100 μg/mL) for 24 h. LPS from *E. coli* (1 μg/mL) was employed as a positive control, and the medium was the negative control. Cell culture supernatant (60 μL) was mixed with Griess reagent (60 μL) and incubated for 5 min in darkness. The absorbance was measured at 540 nm using a microplate reader (TECAN, Safire^2, Austria). The amount of NO was calculated using a calibration curve with various concentrations of sodium nitrite (0.78–100 μM).

2.5.2. Neutral red pinocytosis assay

The cellular pinocytic activity (serving as a proxy for phagocytosis) was assessed using neutral red (NR). Briefly, 0.1 % NR solution was made by solubilizing 0.1 g neutral red crystals in 100 mL sterile phosphate buffer (pH 7.2). The solution was subsequently purified through filtration employing a syringe filter (0.45 μm) for removing insoluble crystals and ensuring homogeneity.

RAW 264.7 cells were prepared in 96-well plates and incubated for 24 h as described in 2.5.1. Test agents were added for 24 h, then 20 μL of 0.1 % NR solution was added to each well for 6 h. Supernatants were carefully aspirated and discarded, and the wells were rinsed twice using 200 μL of PBS. Then 100 μL of cell lysis solution was added (50 % absolute ethanol, 49 % deionized water, and 1 % glacial acetic acid), followed by incubation at R.T. for 2 h. Absorbance was measured at 540 nm using a microplate reader (TECAN, Safire^2, Austria).

2.5.3. Macrophage proliferation assay

RAW 264.7 cells were prepared in 96-well plates and incubated for 24 h as described in 2.5.1. Cells were exposed test agent for 20 h. LPS from *E.coli* (1 μg/mL) served as a positive control, whereas the medium as a negative control. AlamarBlue (10 μL) was added to each well and incubated (4 h) and protected from light. Absorbance was measured at 570 nm, with 600 nm as a reference wavelength (for normalisation) using a microplate reader (TECAN, Safire^2, Austria). Proliferation index was calculated formula: $PI = (A_{sample}\text{-}A_{blank})/(A_{medium}\text{-}A_{blank})$.

2.5.4. Cytotoxicity assay

Cell cytotoxicity was assessed by using an MTT assay kit (Merck®, UK) with cells at a density of 5×10^5 cells/mL in accordance with the manufacturer's protocol, as described in Supplementary Method S4.

2.5.5. Cytokine secretion assay

Several proinflammatory and anti-inflammatory cytokines secretions including IFN-γ, IL-2, IL-1β, IL-4, IL-6, IL-12, TNF-α and IL-10 in the culture supernatant after treating with SC-P50 were determined using the ELISA kits respectively, following the manufacturer's protocol. Briefly, RAW 264.7 cells were cultured, placed into 96-well plates and incubated for 24 h as detailed in 2.5.1. Following a 24 h incubation period at 37 °C with 5 % CO2, the medium from each well was extracted and discarded, 100 μL of serial diluted SC-P50 solution was then added to the wells. LPS from *E.coli* (1 μg/mL) served as the positive control, whereas the medium was employed as the negative control. The plate was subjected to an additional 24 h incubation period at 37 °C with 5 % CO_2 and then ready for cytokines determination by ELISA kits.

2.5.6. Studies in human primary cells

SC-P50 was tested for biological activities using the BioMAP Diversity PLUS panel of 12 human primary cell-based systems (Table S1; Eurofins Discovery, Missouri, USA). These systems have been engineered to simulate intricate human tissue and disease characteristics related to the vascular system, skin, lungs, and inflammatory tissues. Biomarker activities (Table S1) within this diverse array, combined with a comparative evaluation of the biological effects of established bioactive substances present in the BioMAP reference database, serve as a

means to forecast the safety, effectiveness, and functionality of the arabinan.

2.5.7. Determination of IL-8 expression

Since the BioMAP Diversity PLUS panel indicated that IL-8 was increased by SC-P50 in 10 human primary cell-based systems, the expression of IL-8 in IL-8 LucRep-RAW 264.7 cells (Supplementary Method S3) was determined using the luciferase assay reagent kit (2BScientific™, Kirtlington, UK) with a luminometer (CLARIO Star®, Germany) by following the manufacturer's protocol. The experimental procedure is outlined in Supplementary Methods S5.

2.5.8. Inhibitors studies

Several attempts to chemically label SC-P50 by different approaches were unsuccessful yielding derivatives that were devoid of biological activity. This precluded receptor binding studies, and so inhibitors of pattern recognition receptor (PRR) were employed to probe involvement of TLR2, TLR4, Dectin-1 and mannose receptor (MR) in SC-P50's stimulation of NO production and IL-8 expression/secretion in IL-8 LucRep-RAW 264.7 cells. Additionally, inhibitors of intracellular signalling molecules were (NF-κB, IκB-α, MEK/ERK inhibitor; MAPK, JNK and MyD88) were also employed. The inhibitors used and the experimental procedure are outlined in Supplementary Method S6.

2.5.9. Metabolic response studies

To investigate the metabolic responses of RAW 264.7 cells to SC-P50 or fucoidan, metabolomic profiling was undertaken. Briefly, RAW 264.7 cells were introduced onto a 6-well plate containing 2 mL of cell suspension (1×10^6 cells/mL, totalling 2×10^6 cells per well). Following this, the plate was subjected to incubation for a duration of 24 h at 37 °C with 5 % CO_2. The SC-P50 or fucoidan solution, which had been sterilized, was further diluted to concentrations of 1, 10, and 100 μg/mL with cell culture medium. After 24 h incubation, the medium from each well was removed and 2 mL of each diluted arabinan solution was introduced into the respective wells. The medium was employed as the control. Following a 24 h incubation period at 37 °C with 5 % CO_2, the medium was aspirated, and the cells were subjected to two rounds of gentle washing with ice-cold PBS, then 2 mL of PBS was added to each well. The procedure by which cells were detached, intracellular metabolites extracted and measured is outlined in Supplementary Method S7.

2.6. Statistical analysis

Data were shown as means ± standard deviation (SD). Statistical analysis was performed using Graphpad Prism 9.0 software (GraphPad, California, USA), with a one-way ANOVA with Dunnett's multiple Comparison Test comparing treatment groups and control, and significance indicated (*$P < 0.05$, **$P < 0.01$, ***$P < 0.001$, ****$P < 0.0001$).

3. Results

3.1. Extraction of S. cordifolia root powder and preliminary chemical analyses

An extraction protocol (Fig. 1) was devised based on several different attempts to optimize and isolate a pure form the arabinan produced by this plant. These other attempts consisted in the combined use of different chromatographic techniques, such as size exclusion chromatography on (Sephacryl HR-300, Sephacryl HR-100), ion exchange chromatography (Q-Sepharose fast flow), ion hydrophobic chromatography (Octyl-Sepharose), and graphitized carbon on solid phase chromatography. As for the protocol developed, the powdered plant root was treated with 95 % ethanol to remove the lipophilic components (step 1, Fig. 1) and then extracted with hot water (100 °C, step 2, Fig. 1). The supernatant afforded after centrifugation was treated with both amylase and pullulanase (step 3, Fig. 1) since amylopectin-like glycans were found during the preliminary purification trials. The clear solution was made 80 % with ethanol to separate the glycans on the basis of their different solubility in the solution (step 4, Fig. 1). Both the precipitate (SC-P, 50 mg) and the supernatant (SC-P, 17 mg) were inspected by proton NMR (Fig. 2).

The analysis of the proton spectra of the two fractions (Figs. 2 and S1) disclosed the presence of carbohydrate material, due to the signals in the anomeric region (5.3–4.3 ppm) along those in the carbinolic area (4.3–3.0 ppm). However, the anomeric signals had no-apparent stoichiometric ratio, suggesting the presence of a (or of a mixture of) polysaccharide with a non-repetitive unit, like often occurs in plant polysaccharides (Gorshkova et al., 2013).

To acquire more information, monosaccharide composition analysis was performed, and it disclosed that both fractions contained almost the same type of monosaccharides, albeit in different proportions (Fig. S2) as judged by the intensities of the peaks in the two chromatograms. In particular, the presence of galacturonic acid and rhamnose suggested the presence of a pectic-like glycan, while the occurrence of arabinose and galactose suggested that an arabinogalactan could be present. Other monosaccharides, like glucose, xylose (in traces at 8.2 min.) suggested that glucans and/or hemicellulose-like glycans could be part of the mixture. These chemical data supported the notion that SC-P and SC-S were mixtures of different glycans, and additional purification trials (step 5, Fig. 1) were conducted to separate them and to remove the contaminants that were visible in the high- and low-field regions of the proton spectra (Fig. S1).

3.2. Purification of SC fractions by solid phase extraction

SC-P and -S were further separated by using a graphite-based adsorbent (step 5, Fig. 1). This matrix is mostly used for the separation of discrete size oligosaccharides (Koizumi, 2002), and it seems that separation is driven by hydrophobic interactions. In order to make the separation scalable and in high throughput manner, a SPE cartridge was used instead of a HPLC column. TFA or other organic acids were not used in contrast to what devised in many protocols, to avoid the cleavage of labile glycosidic linkages like those of the furanose residues.

The different fractions were analysed by proton NMR (Fig. 3) and the first result noted was the decrease in the level of contaminants (Figs. S3 and S4). All fractions lost the initial brownish colour which probably remained adsorbed on the cartridge, as also supported by the fact that the total sample recovery did not match the initial amount of sample loaded. For SC-S, the recovery yield was 65 % (~ 11 mg recovered over 17 mg loaded) while for SC-P it was 75 % (~ 18 mg recovered over 25 mg loaded).

The fractions from 0 to 40 % ACN (except SC-S40) presented quite broad signals, still non-carbohydrate signals in the high-field region (Figs. S3 and S4) and non-stoichiometric ratio between the anomeric signals. On the contrary, the fractions recovered with 50 % ACN (SC-P50 and SC-S50) had four main anomeric signals (5.4–5.20 ppm) in an almost 1:1 ratio and almost no contaminants. Based on these findings, these two fractions were characterized in more detail.

3.2.1. Molecular weight and linkage analysis

SEC-HPLC determined the average molecular weight (MW) of the SC-P50 and SC-S50 by calibrating the column with a set of dextran standards of known molecular weight (Fig. S5). The calibration line was determined by fitting the experimental points by linear regression, and the equation $Log_{MW} = -0.7105 \times t + 10.813$ ($R^2 = 0.9992$, with "t" = elution time in minutes) was used to determine the molecular weight of the two SC fractions. SC-P50 (66 kDa) had a MW higher than that of SC-S50 (3.2 kDa), in agreement with its lower solubility in cold ethanol. There was very substantial overlap in both proton and HSQC (Fig. S6) spectra profiles, and therefore SC-S50 (the oligosaccharide) and SC-P50 (the polysaccharide) were considered structurally identical, the main

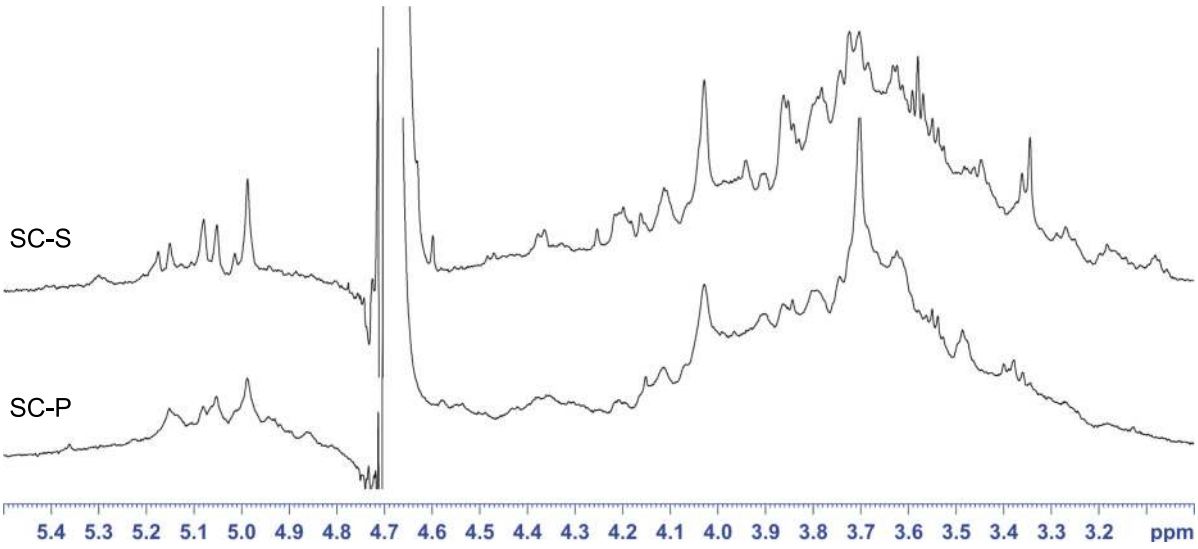

Fig. 2. (600 MHz, 298 K) Expansion of the ^{1}H NMR spectra of the fractions afforded at step 4 (Fig. 1) of *S. cordifolia* root powder purification. The precipitate (SC-P) and the soluble fractions (SC-S) recovered after 80 % ethanol precipitation are reported at the bottom and at the top of the figure, respectively. The full range spectra (Fig. S1) report the presence of non-carbohydrate material at both low and high field.

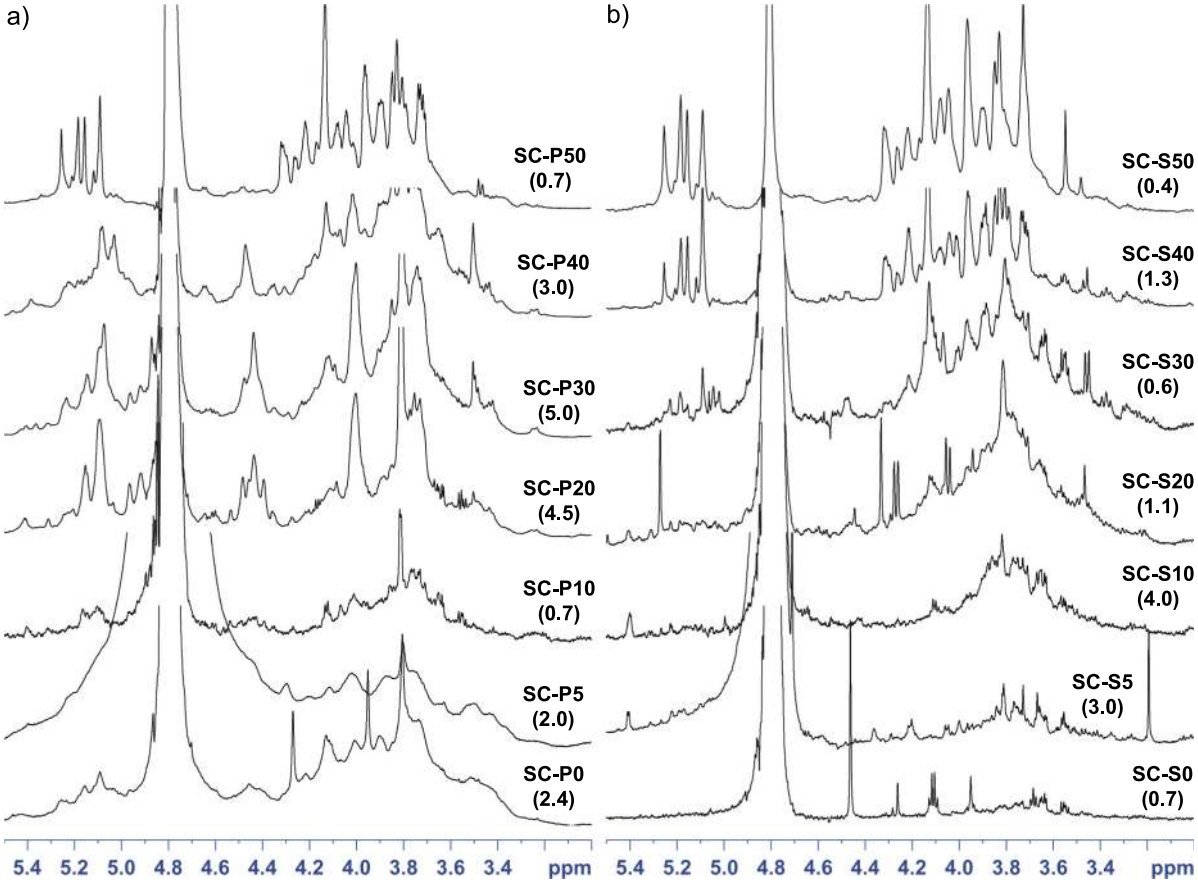

Fig. 3. (600 MHz, 298 K) ^{1}H NMR spectra of the fractions deriving from a) SC-P and b) SC-S by purification with graphite-based SPE (step 5 in Fig. 1). The elution was performed by varying the ACN content of the eluent whose percentage is indicated at the side of the acronym. The numbers in brackets report the amounts (in mg) recovered by the purification. The full range ^{1}H NMR spectra are reported in Fig. S3 for SC-P, and Fig. S4 for SC-S.

difference being the molecular weight. Linkage analysis was tried on both fractions, but it did not lead to any result since the chromatogram did not contain peaks with recognizable fragments. Accordingly, the structural elucidation relied only on the NMR data.

3.2.2. NMR spectroscopy analysis of SC-S50

The full set of 2D NMR spectra was measured by using SC-S50. This fraction was preferred to SC-P50 because it was expected to generate better resolved NMR spectra due to its lower molecular weight.

The analysis of the anomeric region (Fig. 4a, chemical shifts in

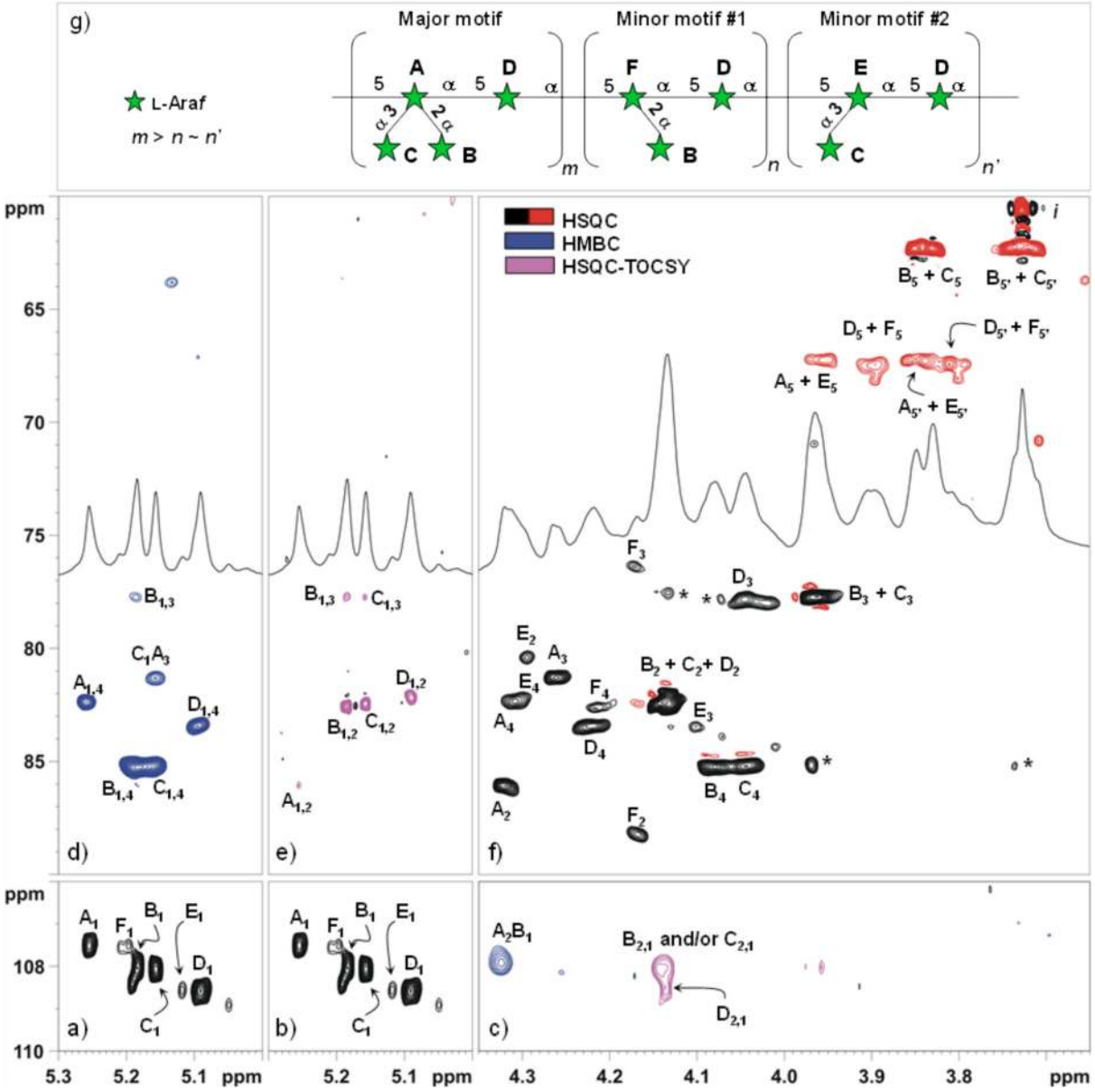

Fig. 4. (^{1}H 600 MHz, ^{13}C 150 MHz, 298 K) ^{1}H—^{13}C NMR spectra recorded for SC-S50 arabinan (or SCA). Expansions of the HSQC spectrum (black densities for the carbinolic carbon atoms and red densities for the hydroxymethylene carbons) are displayed in panels a, b and d. The HMBC spectrum (blue densities) is reported in panels c and d, while the HSQC-TOCSY (pink densities) is reported in panels c (in overlay with the HMBC) and e. The full HSQC spectrum is given in Fig. S7, and the labels correspond to the residues listed in Table 1 or in panel g. g) structure of SC-S50 or SCA, elaborated on the basis of the NMR data. The densities marked with "*" are COSY-artifacts of the HSQC sequence (Speciale et al., 2022). "*i*" stands for impurity.

Table 1) disclosed the presence of four main signals, labelled **A** – **D**, in almost 1:1 ratio along with others of lesser intensity, all associated to carbon chemical shifts at about 108 ppm (Table 1), diagnostic of residues in the furanose form (Speciale et al., 2022). Starting from the anomeric protons, the HSQC-TOCSY (Fig. 4e) reported the presence of one density in the carbinolic region for each signal, with **B** and **C** also displaying a second density of minor intensity. Since the magnetization transfer in the HSQC-TOCSY sequence follows the sequence of the protons over the monosaccharide ring (*e.g.* H-3 cannot be detected if H-2 is not detected first) and it decreases for protons that are far along the sequence, the intense correlations were assigned to the C-2 of the units (labelled as $\mathbf{B_2}$ and $\mathbf{C_2}$, respectively), while those less intense of **B** and **C** to their C-3. The position of the carbinolic protons was determined by integrating the information of the homonuclear spectra (Fig. 5b). The COSY spectrum enabled the finding of the H-2 protons of each unit (Fig. 5b) so that the correct C-2 density was labelled in the HSQC spectrum (Fig. 4f). Regarding **A**, H-2 had no apparent correlation with H-3 in the COSY spectrum, but the position of this proton was evaluated by TOCSY spectrum because it connected H-1 of **A** to a signal at 4.26 ppm, which in turn had a COSY correlation with a proton at 4.31 ppm, next but not coincident to H-2 (note the grey lines in Fig. 5d). The proton at 4.31 ppm had a carbon at 82.3 ppm, which in turn correlated with the anomeric proton of **A** in the HMBC spectrum (Fig. 4d). Based on this finding, the density at ^{1}H/^{13}C 4.31/82.3 ppm was assigned to $\mathbf{A_4}$, since this C-4 displayed the long-range correlation with the anomeric proton because involved in the ring closure, as deduced by the corresponding density, labelled $\mathbf{A_{1,4}}$ (Fig. 4d) in the HMBC spectrum.

Then, H-4 displayed three correlations in the COSY spectrum: that with H-3 and other two (3.95 and 3.84 ppm) which were assigned to H-5 and H-5′ of the residue (or $\mathbf{A_{4,5}}$ and $\mathbf{A_{4,5'}}$, Fig. 5d), since both correlated to a hydromethylene carbon atom at 67.2 ppm in the HSQC (labelled $\mathbf{A_5}$, Fig. 4f).

Table 1
Proton (600 MHz) and carbon NMR chemical shifts (150 MHz) (Acetone as internal standard, ^{1}H 2.225, ^{13}C 31.45 ppm), deduced for SC-S50 arabinan isolated from *S. cordifolia*.

Residue	Nucleus	1	2	3	4	5
A	^{1}H	5.26	4.33	4.26	4.31	3.95; 3.84
2,3,5-α-Araf	^{13}C	107.4	86.0	81.3	82.3	67.2
B	^{1}H	5.19	4.13	3.97	4.09	3.73; 3.84
t-α-Araf	^{13}C	108.0	82.4	77.7	85.1	62.2
C	^{1}H	5.16	4.14	3.97	4.04	3.73; 3.84
t-α-Araf	^{13}C	108.0	82.4	77.7	85.0	62.2
D	^{1}H	5.09	4.13	4.05	4.23	3.89; 3.80
5-α-Araf	^{13}C	108.5	82.4	77.8	83.4	67.6
E	^{1}H	5.12	4.29	4.10	4.31	3.95; 3.84
3,5-α-Araf	^{13}C	108.6	80.4	83.3	82.3	67.2
F	^{1}H	5.20	4.16	4.17	4.21	3.89; 3.79
2,5-α-Araf	^{13}C	107.5	88.2	76.4	82.5	67.9

Collectively, these data indicated that **A** was a pentose in the furanose form, which based on the monosaccharide composition (Fig. S2) was assigned to an arabinose unit since this was the only pentose detected in the mixture. Its L absolute configuration was assumed on the basis that plants only produce this isomer (Kotake et al., 2016). Finally, the C-1 chemical shift value (107.4 ppm) indicated the α configuration of the anomeric centre, while the low field shifted values of C-2 (86.0 ppm), C-3 (81.3 ppm) and C-5 (67.2 ppm) disclosed that **A** was substituted at all the available positions (Speciale et al., 2022).

Regarding **B** and **C**, the F1 dimension of the TOCSY spectrum (Fig. 5c) defined the position of all the protons, overcoming the limits related to the severe overlap between $\mathbf{B_2}$ (4.13 ppm) and $\mathbf{C_2}$ (4.14 ppm), $\mathbf{B_3}$ and $\mathbf{C_3}$ (both at 3.97 ppm) and their H-5 s, identifying their H-4 s ($\mathbf{B_4}$ and $\mathbf{C_4}$) at 4.09 and 4.04 ppm, respectively. Differently from **A**, **B** and **C** were two α-arabinofuranose units non-substituted, namely they occurred as terminal units (Speciale et al., 2022). The identification of the proton/carbon chemical shifts of **D** followed the same strategy used for the other units. The COSY correlation identified $\mathbf{D_2}$ at 4.13 ppm (Fig. 5b), namely clustered with $\mathbf{B_2}$ and $\mathbf{C_2}$, but the TOCSY density at 4.05/5.09 ppm (Fig. 5b) determined the position of $\mathbf{D_3}$, then the other protons were found by following the connections dictated by the COSY spectrum (Fig. 5d), while HSQC analysis returned the corresponding carbon values. Accordingly, **D** was a α-arabinofuranose unit only substituted at *O*-5 (C- 5 at 67.6 ppm, Fig. 4f). The analysis of the residues with lesser intensity was possible by raising the levels of the homonuclear spectra (Figs. S8 and S9) and it led to the assignment of only two of them, **E** (H-1 at 5.12 ppm) and **F** (H-1 at 5.20 ppm). As for **E**, its $\mathbf{E_2}$ (4.30

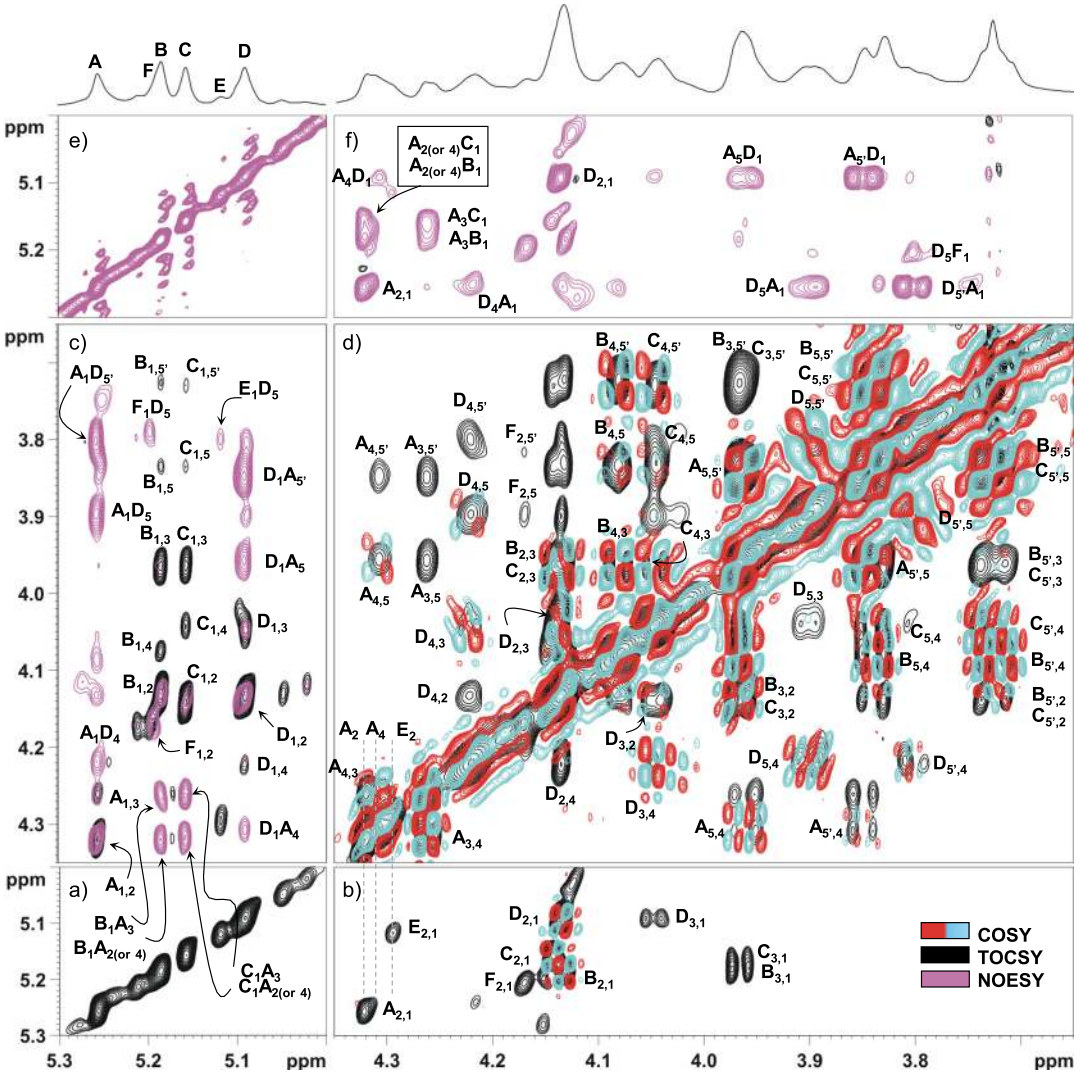

Fig. 5. (600 MHz, 298 K) ^{1}H—^{1}H NMR spectra recorded for SC-S50 arabinan (or SCA). Suitable expansions of the COSY spectrum (red and cyan densities) are displayed in panels d, and e. The TOCSY spectrum (black densities) is reported in panels a - d, while the NOESY spectrum (pink densities) is reported in panels c (in overlay with the TOCSY), e and f. The two grey dotted lines in panel d indicate the exact position of H-2 and H-4 of **A**. The labels correspond to the residues listed in Table 1.

ppm, Fig. S8) had a TOCSY correlation with a proton at 4.10 ppm, labelled **E_3**, whose carbon (80.4 ppm, Fig. 4f) was glycosylated. Then, H-3 of **E** had one TOCSY correlation with a proton at 3.95 ppm (Fig. S8) which crossed two carbon densities at 77.8 and 67.2 ppm in the HSQC spectrum. The possible match with the density at 77.8 ppm was excluded since C-4 of an arabinofuranose unit never reaches such a high field value even when the neighbouring positions are substituted. Accordingly, the proton at 3.95 ppm was matched with the hydroxymethylene carbon at 67.2 ppm with the consequence it had to be assigned to **E_5**. The position of H-4 was then assumed to coincide with that of H-2 while the corresponding H-4/C-4 density was defined as coincident with that of **A_4** in the HSQC spectrum (Fig. 4f).

Regarding **F**, H-1 (5.20 ppm, Figs. 5b and S8) was connected to a proton at 4.16 ppm which in turn had other three correlations with the protons at 4.21, 3.89 and 3.79 ppm (Fig. S8). These last two protons correlated with the hydroxymethylene carbon at 67.9 ppm (Fig. 4f), therefore were assigned to H-5 and H-5′ of **F**, respectively. Then, the proton at 4.16 ppm crossed with two different carbon atoms at 88.2 and 76.2 ppm in the HSQC spectrum (Fig. 4f). Based on the carbon chemical shifts values reported for the corresponding methylglycoside (C-2 at 81.8, C-3 at 77.5, C-4 at 84.9 ppm) and taking into account the chemical shifts variations due to the glycosylation effects (6 to 10 ppm for the α-effect, 0 to - 3 ppm for the β-effect) (Speciale et al., 2022), both densities were assigned to **F** as **F_2** and **F_3**, respectively, while the other proton left at 4.21 ppm, was assigned to H-4 in turn connect to a carbon at 82.5 ppm (Fig. 5f). Thus, **F** was a α-arabinofuranose 2,5-linked, while **E** was 3,5-linked.

Finally, the HMBC and NOESY spectra disclosed the sequence between the different units. First, **C** was placed on *O*-3 of **A** based on the **C_1A_3** correlation in the HMBC spectrum (Fig. 4d), so that the HMBC density at $^1H/^{13}C$ 4.33/108.0 ppm could be assigned to **A_2B_1** instead of **A_2C_1** (Fig. 4c). The NOESY then correlated H-1 of **A** (Fig. 5f) to **D_5** and **D_5'**, namely the sequence **A**-(1 → 5)-**D**, in agreement with the displacement at low field found for C-5 of **D**, the correlation **A_1D_4** instead arose by the spatial proximity between the two protons. Then, the NOE effects **A_5D_1** and **A_5'D_1** (Fig. 5f) indicated that **D** was attached to *O*-5 of **A**.

Regarding the location of **E** and **F**, both had a correlation with H-5′ of **D** (Fig. 5c, Fig. S9), meaning that they occupied a position equivalent to that assigned to **A**. This apparent contradiction was solved by making the hypothesis that the glycosylation on the **A** residues was not complete and that when the substituent at *O*-3 was absent, the residue detected was **F**, while if only *O*-3 was substituted the residue detected was **E**. The analysis of the NOESY spectrum with an increased number of levels (Fig. S9) determined also that substituents located at *O*-3 and *O*-2 of **E** and **F**, respectively, which were coincident with the previously defined **C** and **B** units, respectively.

Thus, combining the information from all the NMR data, it was possible to recognize the presence of three distinct structural motifs. The main motif consisted of the arabinofuranose **A** – **D** units, connected through α-(1 → 5) linkages with **A** further substituted at *O*-2 and *O*-3 with **B** and **C**, respectively (Fig. 4g). Beside this major structural unit, it was possible to recognize other two minor motifs, apparently in similar proportions and involving **E** and **F**, which replaced the unit **A** of the main backbone, or that could be considered as deriving by its incomplete glycosylation. Due to the heavy overlap of the NMR signals, it was not possible to estimate the between the different anomeric protons, and due to the lack of linkage analysis, it was not possible to establish the relative ratio between the different motifs. Given the equivalence of the proton spectra of SC-S50 and SC-P50 (Fig. S2), these were considered having the same arabinan with the only difference being the molecular weight and for both, the acronym SCA (*S. cordifolia* arabinan) was adopted.

3.3. In vitro experiments of SCA

3.3.1. NO production determination on RAW 264.7 cells

At each stage during the optimization of the arabinan's isolation (as described in Section 3.1) the bioactivity was monitored by measuring the ability of fractions to activate macrophages *in vitro*. This involved measuring concentration-dependent (3.125 μg/mL to 100 μg/mL) effects on cellular NO production in RAW 264.7 cells and then focusing extraction studies on fractions of increased activity. Fig. 6 shows the performance of the fractions that were ultimately arrived at in the flow chart in Fig. 1. SC-P50 (high molecular weight) markedly increased the NO production in RAW 264.7 cells compared with the control (culture media). This occurred in concentration-dependent manner (15.92 ± 1.36 μM to 68.28 ± 4.04 μM). By comparison, the NO production of SC-S50 (low molecular weight) was negligible, reaching 2.18 ± 0.18 μM at 100 μg/mL. During further confirmatory testing the EC_{50} for SC-P50 for NO production was determined to be 7.92 μg/mL (Fig. S10a).

3.3.2. Effects of SC-P50 on proliferation, pinocytic activity and viability in RAW 264.7 cells

The proliferation index results indicated that SC-P50 stimulated RAW 264.7 cells proliferation in a concentration-dependent manner from 1.23 to 300 μg/mL (Fig. 7a). SC-P50 significantly enhanced the pinocytic activity of RAW 264.7 cells when it ranged from 12.5 to 100 μg/mL (Fig. 7b). SC-P50 increased the membrane projections and number of vacuoles of RAW 264.7 cells in internalising pathogens. SC-P50 did not reduce cell viability at concentrations of 333.3 μg/mL and below (Fig. 7c). However, viability was significantly reduced at 1000 μg/mL.

3.3.3. Effects of SC-P50 on cytokine secretion from RAW 264.7 cells

In Fig. 8, SC-P50 stimulated strong concentration-dependent secretion of IL-6 and TNF-α from RAW 264.7 cells. The production of IL-6 in RAW 264.7 cells was above 400 pg/mL when the cells were treated with 25–100 μg/mL of SC-P50 for 24 h. The production of TNF-α in RAW 264.7 cells ranged from above 2000–5000 pg/mL when the cells were exposed to SC-P50 doses ranging from 3.125 to 100 μg/mL. SC-P50 only had weak stimulatory activity on IL-2 secretion, and this only occurred at the highest concentration tested (100 μg/mL; Fig. 8a). SC-P50 did not increase the secretion of IFN-γ, IL-1β, IL-4, IL-12 or IL-10 from RAW 264.7 cells (Fig. S11).

3.3.4. Results of screening of SC-P50 using the BioMAP diversity PLUS panel of 12 human primary cell-based systems

In Fig. 9a, SC-P50 is active with >50 annotated readouts which are outlined fully in Table S2.

SC-P50 was antiproliferative to endothelial cells (3C system), human primary T-cells (SAg system), coronary artery smooth muscle cells (CASM3C system), and fibroblasts (HDF3CGF system). SC-P50 was non-toxic in all cell systems at concentrations up to 100 μg/mL.

SC-P50 impacted inflammation-related activities as indicated by its ability to decrease Eotaxin 3, MCP-1, I-TAC, MIG, ICAM-1 and IP-10; and to increase MIP-1α, IL-8, IL-6; modulated VCAM-1 and IL-1α. There was clear evidence of immunomodulatory activities (decreased M-CSF, sIL-2; and increased sIL-17A, sIL-6, sIL-17F), and tissue remodelling activities (decreased Collagen I, Collagen IV, uPA, PAI-1, MMP-9, bFGF; increased TIMP-2, TIMP-1, MMP-1, MMP-3, uPAR).

SC-P50 increased secreted IgG, sIL-17A, sIL-17F, sIL-2, sIL-6, and TNF-α in BT system. However, SC-P50 diminished IgG and sIL-17F secretion at higher test concentrations (100 μg/mL), and sIL-2 secretion at lower concentration (1, 10 μg/mL) in the same systems (Fig. 9b).

Very notably, SC-P50 decreased MIG in 3C, SAg, BE3C, CASM3C, HDF3CGF, and KF3CT systems (Fig. 9c).

Also, very notable it was the increased IL-8 in 3C, LPS, SAg, BF4T, BE3C, CASM3C, HDF3CGF, KF3CT, MyoF and /Mphg systems (Fig. 9d). This finding led to the secretion/expression of IL-8 being investigated in

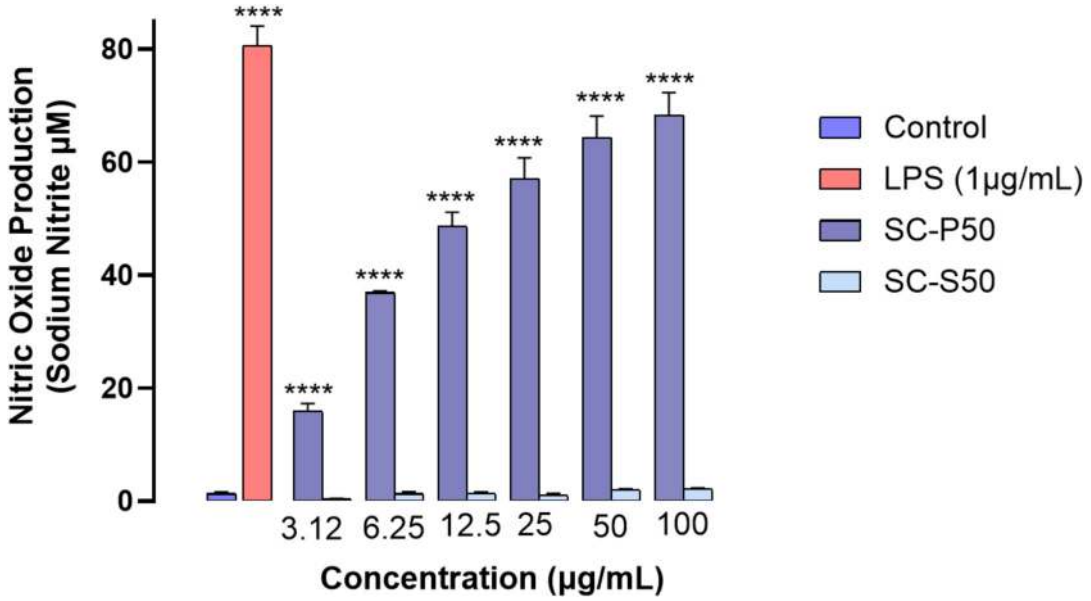

Fig. 6. NO production of polysaccharide fractions (SC-P50 and SC-S50) in RAW 264.7 cells. The figure shows the concentration-dependent (NO) production stimulated by the high (SC-P50) and the low (SC-S50) molecular weight arabinan structures, along with a negative control (culture media) and a positive control LPS (1 μg/mL). $^{****}P < 0.0001$ compared with medium control.

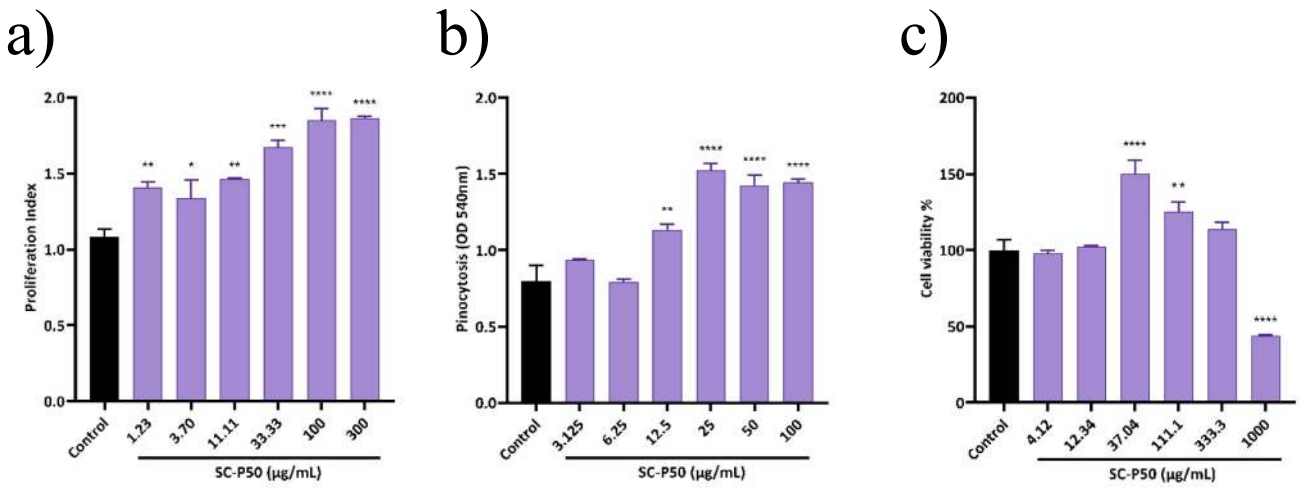

Fig. 7. Cell culture results. a). Proliferation index of SC-P50 on RAW 264.7 cells, b). Pinocytosis of SCA on RAW 264.7 cells as measured by neutral red. The OD was assessed at 540 nm using a microplate reader, c). MTT assay of SC-P50 on RAW 264.7 cells. $^{*}P < 0.05$, $^{**}P < 0.01$, $^{***}P < 0.001$ and $^{****}P < 0.0001$ compared with medium group.

RAW264.7 cells.

An unsupervised search for mathematically similar compound profiles was performed against the BioMAP Reference Database (Fig. 9e). The profile of SC-P50 (100 μg/mL) was most closely aligned to fucoidan (37 μg/mL) with 31 common activities between SC-P50 and fucoidan as listed in Table S2.

Using the BioMAP analysis it was also possible to assess the effects of SC-P50 on cells with an either M1 or M2 phenotype. SC-P50 was active in both the 'M1-like' 3C system (HUVEC cells pre-treated with IL-1β, TNFα and IFN-γ; *i.e.*) and the 'M2-like' 4H system (HUVEC cells pre-treated with IL-4 and histamine (Fig. S12).

3.3.5. Inhibitor studies of NO production mechanisms in IL-8 LucRep-RAW 264.7 cells

In Fig. 10a, the findings of the inhibitor studies revealed that the inhibitor TAK 242, which targets TLR4, significantly impeded the arabinan-stimulated production of NO, to levels comparable to those observed in the medium control group. Conversely, other inhibitors targeting PRRs did not demonstrate notable inhibition of NO production. This suggests that TLR4 has a vital role in recognizing SC-P50 by IL-8 LucRep-RAW 264.7 cells. All inhibitors targeting NF-κB pathways, including PDTC, TPCK, and BAY 117082 (Fig. 10b), significantly diminished the SC-P50-stimulated NO production, indicating that arabinan activates RAW 264.7 cells *via* NF-κB pathways. Additionally, in Fig. 10c, SP600125, a selective inhibitor of the JNK pathway, significantly impeded the SC-P50-induced NO production, suggesting that JNK is involved in SC-P50 signal transduction in macrophages. In Fig. 10d, the inhibitory peptide for MyD88 signalling did not exhibit any significant inhibition of NO production, indicating that SC-P50-mediated intracellular signal transduction may occur *via* the MyD88-independent pathway. Furthermore, in Fig. 10e and f, mianserin and MD-2 antibody, which target TLR4's extracellular domain and cofactors,

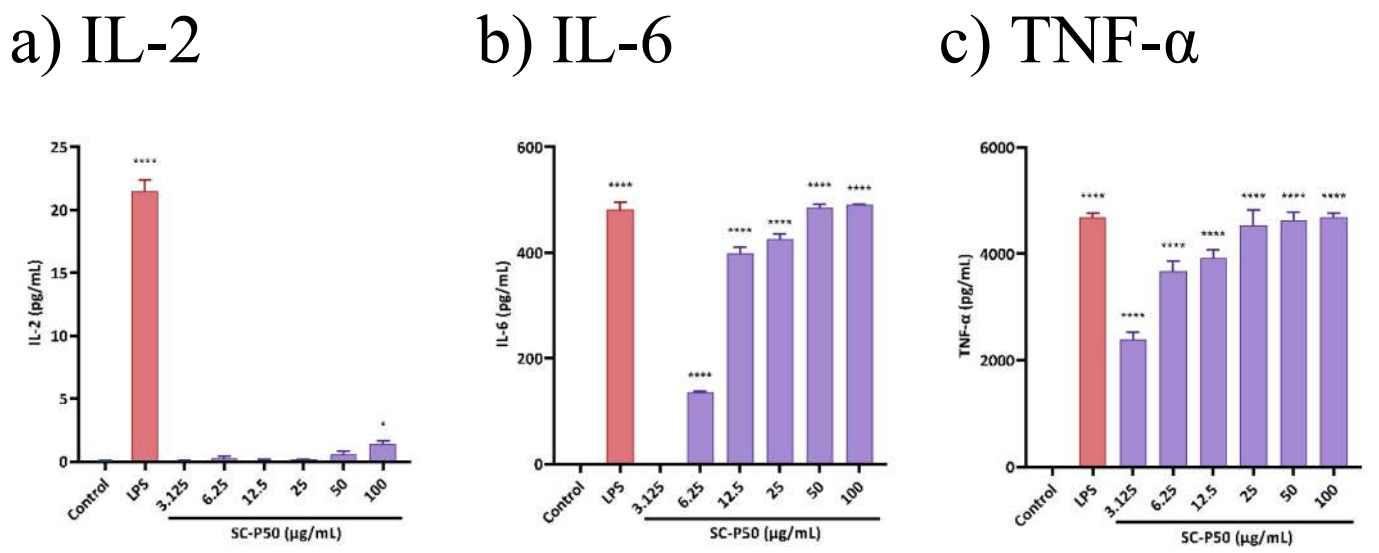

Fig. 8. Secretion of a). IL-2, b). IL-6, and c). TNF-α as stimulated by SC-P50 in RAW 264.7 cells measured by ELISA kits. *P < 0.05 and ****P < 0.01 compared with Control (medium).

significantly reduced the SC-P50-stimulated NO production, indicating that SC-P50 can bind to the extracellular domain of TLR4 and induce the activation of RAW 264.7 cells.

3.3.6. *IL-8 expression determination on IL-8 LucRep-RAW 264.7 cells*

As shown in Fig. 11a. SC-P50 exhibited a notable concentration-dependent increase in the IL-8 expression index on IL-8 LucRep-RAW 264.7 cells compared with control.

3.3.7. *Inhibitor studies of IL-8 producing mechanisms in IL-8 LucRep-RAW 264.7 cells*

In Fig. 11b, the results of the study revealed that inhibitors containing TL2-C29, TAK242, laminarin, and mannan significantly inhibited the arabinan-stimulated IL-8 expression index in IL-8 LucRep-RAW 264.7 cells, but the specific PRR involved was not clear. To investigate this further, the secretion of IL-8 was measured using the mouse IL-8 ELISA kit in the presence of different PRR inhibitors (Fig. S13). The findings revealed that the inhibitors of dectin-1 and TLR4 significantly suppressed the SC-P50-induced up-regulation of IL-8 secretion in IL-8 LucRep-RAW 264.7 cells. Thus, it could be concluded that TLR4 played a crucial role in this process, with dectin-1 also implicated. In Fig. 11c, the BAY 117082 inhibitor, which targets IκBα phosphorylation, significantly reduced the IL-8 expression index, indicating that the NF-κB pathway was involved in the SC-P50-induced up-regulation of IL-8 in IL-8 Luciferase reporter RAW 264.7 cells. Conversely, the MAPK pathway inhibitors and MyD88 signalling inhibitory peptide did not exhibit any significant inhibition of IL-8 expression (Fig. 11d and e), indicating that the SC-P50-induced up-regulation of IL-8 was mediated by the MyD88-independent pathway and that the MAPK pathway was not involved in IL-8 Luciferase reporter RAW 264.7 cells. In Fig. 11f, the TLR4's ectodomain inhibitor, mianserin, significantly lowered the IL-8 secretion index, indicating that the TLR4 extracellular domain binding with SC-P50 contributes to the SC-P50-induced up-regulation of IL-8 expression. The potential involvement MD-2 and/or CD-14 at the TLR4 receptor could not be confirmed because the neutralising antibodies markedly increased IL-8 expression (Fig. 11g). Despites this, the same anti-MD-2 antibody does appear to suppress SC-P50-induced secretion of IL-8 from RAW cells (Fig. S13).

3.3.8. *Metabolic responses to SC-P50 treatment*

The metabolic responses of RAW 264.7 cells to either SC-P50 or fucoidan differed substantially from vehicle control (Fig. S14). Although the metabolic responses of RAW 264.7 cells to SC-P50 and fucoidan were more separated at 100 μg/mL, responses of RAW 264.7 cells to SC-P50 and fucoidan at 10 μg/mL were similar to one other. Fucoidan treatment (1 μg/mL) results in less variability compared to SC-P50 treatment (1 μg/mL), as indicated by the tighter clustering on the PCA plot. Concentration changes of some amino acids, polyamines, glycolysis related metabolites, acylcarnitines and fatty acids are displayed in Fig. S15.

Fig. 12 shows volcano plots generated for SC-P50 (Fig. 12a) and fucoidan (Fig. 12b). These display averaged fold-change differences from the vehicle control at all treatment concentrations (1, 10 and 100 μg/mL). Significantly increased metabolites are shown in red and decreased metabolites are shown in blue. A total of 70 metabolites were significantly increased with SC-P50 treatments, and 37 with fucoidan treatments. There were 35 metabolites significantly decreased with SC-P50 treatments, and 54 with fucoidan treatments. There was considerable overlap between SC-P50 and fucoidan responses (Fig. 12c) with 34 metabolites commonly increased and 16 commonly decreased.

4. Discussion

This study identified and structurally elucidated compounds from the root of *Sida Cordifolia* responsible for this plant's potent immunomodulatory activity (Iqbal et al., 2022). This perennial subshrub of the mallow family produces a distinctive arabinan structure containing specific arabinofuranose motifs. This arabinan exists both in low and high molecular weight forms, and the larger form (SC-P50) possesses highly specific and potent immunological actions. In microgram amounts SC-P50 concentration-dependently activates RAW 264.7 macrophage cells (NO production and phagocytosis). SC-P50 also stimulates proliferation and the secretion of at least four cytokines. SC-P50 is non-toxic, only inducing cytotoxicity at extremely high concentrations (≥1000 μg/mL). At such concentrations proliferation and cytotoxicity differed, perhaps reflecting the differing metabolism of the assay reagents (resazurin: mitochondrial and cytoplasmic; MTT: primarily mitochondrial).

SC-P50's actions are both pro- and anti-inflammatory in nature. The polysaccharide induces profuse secretion of pro-inflammatory IL-6 and TNF-α (Gonzalez Caldito, 2023; Jang et al., 2021; Kaur et al., 2020; Tanaka et al., 2014), but on the other hand, it induces the secretion of IL-2 and IL-8, which are both pro- and anti-inflammatory (Banchereau et al., 2012; Bickel, 1993; Leonard et al., 2024; Qazi et al., 2011; Sharma et al., 2011). SC-P50 induced 50 annotated readouts across 12 human

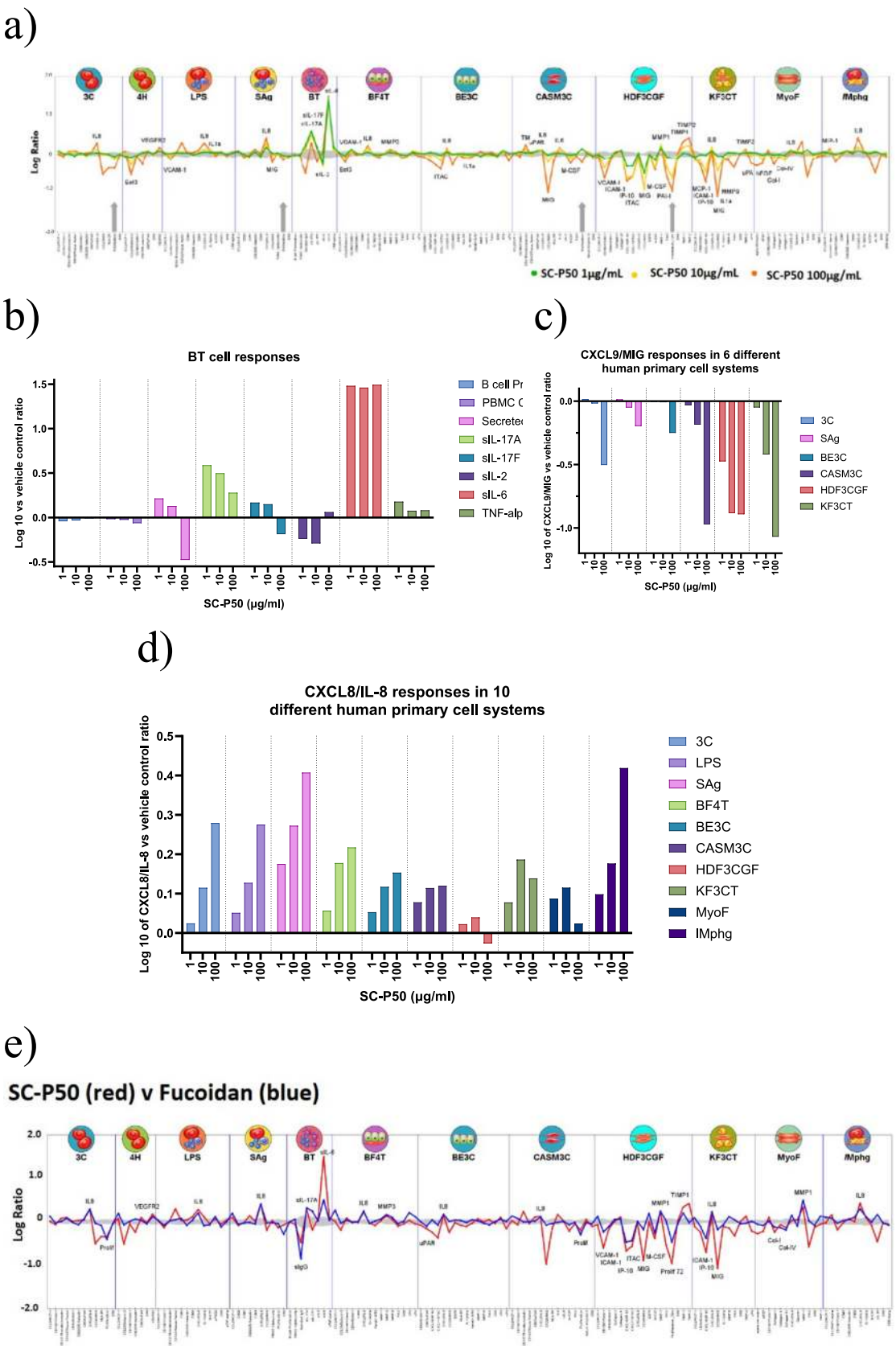

Fig. 9. Findings of screening of SC-P50 using the BioMAP Diversity PLUS panel of 12 human primary cell-based systems. a). BioMAP profile of SC-P50 at three concentrations (1, 10 and 100 µg/mL) obtained from the Diversity PLUS panel in 12 cell-based systems, b). BT system responses to SC-P50, c). CXCL9/MIG responses to SC-P50 in 6 different cell systems, d). CXCL8/IL-8 responses to SC-P50 in 10 different cell systems. e) The BioMAP profile of SC-P50 (100 µg/mL) against fucoidan (37 µg/mL), which was the closest database match.

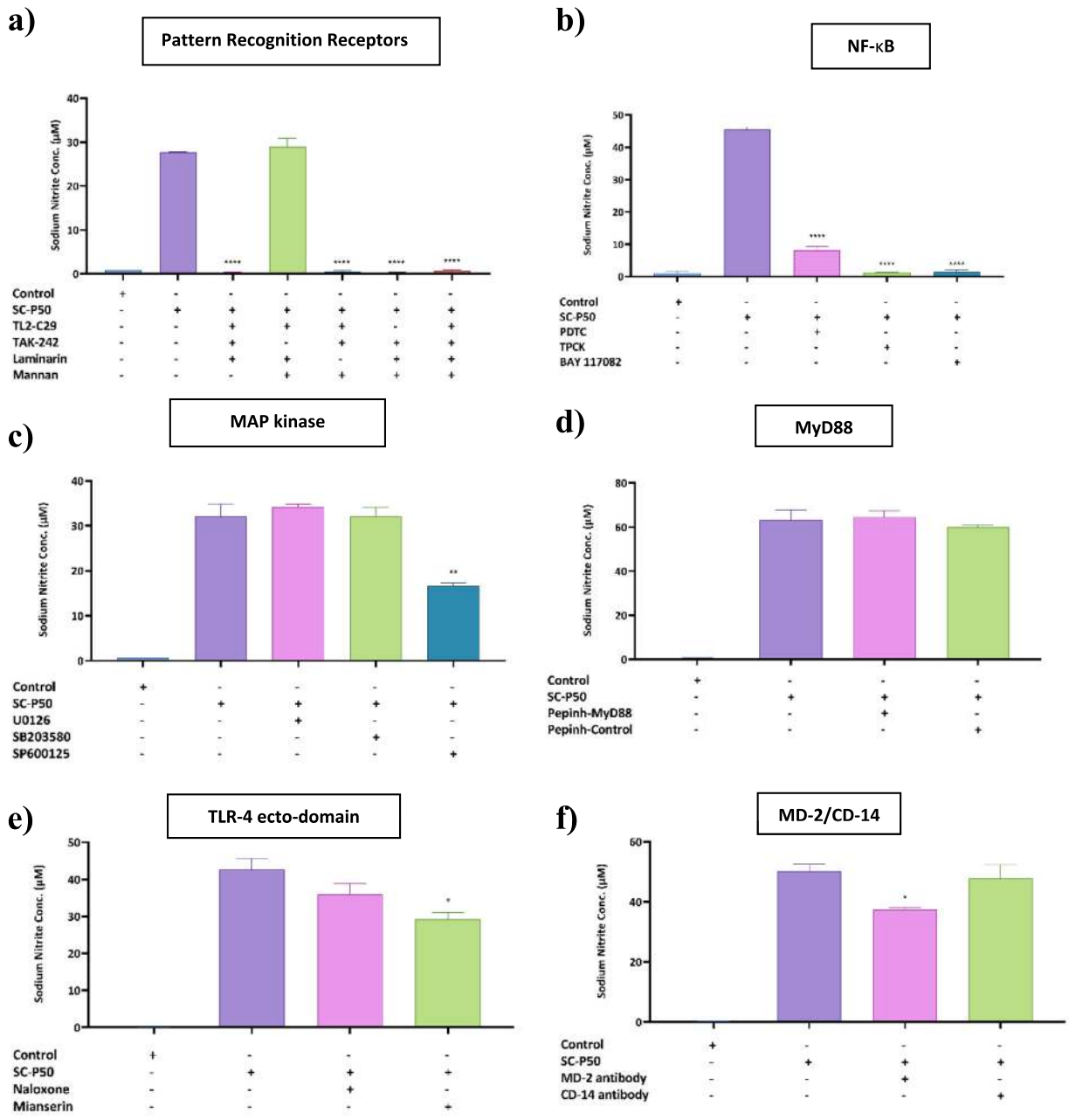

Fig. 10. Effect of pathway inhibitors on the NO production of SC-P50 (100 μg/mL) with different inhibitors in IL-8 LucRep-RAW 264.7 cells. a). pattern recognition receptor inhibitors for TLR2 (TL2-C29: 5 μg/mL); TLR4 (TAK-242: 5 μg/mL); Dectin-1 (laminarin: 300 μg/mL) and MR (mannan: 200 μg/mL). b). NF-κB pathway inhibitors (PDTC: 300 μM; TPCK: 30 μM; BAY 117082: 30 μM), c). MAPK pathway inhibitors (U0126: 10 μM; SB203580: 20 μM; SP600125: 20 μM), d). MyD88 signalling pathway inhibitors (Pepinh-MyD88: 10 μM; Pepinh-MyD88: 10 μM), e). TLR4 ecto-domain inhibitors (naloxone: 100 μM; mianserin: 100 μM), f). TLR4's extracellular domain cofactors antibodies (MD-2 antibody: 5 μg/mL; CD-14 antibody: 10 μg/mL). $^{*}P < 0.05$, $^{**}P < 0.01$ and $^{****}P < 0.0001$ compared with the SC-P50 treatment group.

cell systems, and therefore its actions are not confined to macrophages. A remarkable, near universal, augmentation of human IL-8 is a central feature of SC-P50's bioactivity. IL-8 has two key functions. Firstly, inducing chemotaxis in target cells (neutrophils & granulocytes) migrating them to a site of infection. Secondly, it stimulates phagocytosis once these have arrived at the site of infection (David et al., 2016).

Human cell studies also confirmed SC-P50's observed augmentation of IL-6 and IL-2 secretion, revealed that it also modulates IL-17, immunoglobulin G (IgG) and various chemokines. SC-P50's suppression of the chemokine MIG (monokine induced by gamma interferon (CXCL9) was highly consistent across cell types. MIG is involved in regulating immune cell migration, differentiation and activation (Tokunaga et al., 2018). Therefore, SC-P50 has profound immunomodulatory effects both up- and down- regulating key signalling proteins of the immune system.

SC-P50's cellular mechanisms of action were probed by two approaches. First, using various receptor/pathway inhibitors, and second, by metabolomic profiling to understand its impact on macrophage cell metabolism. These results further support SC-P50's actions being both pro-inflammatory and anti-inflammatory. TLR4 is at least one of the cognate receptors for SC-P50, and the TLR4-NF-κB pathway appears pivotal for its stimulation of NO production. TLR4 is partially

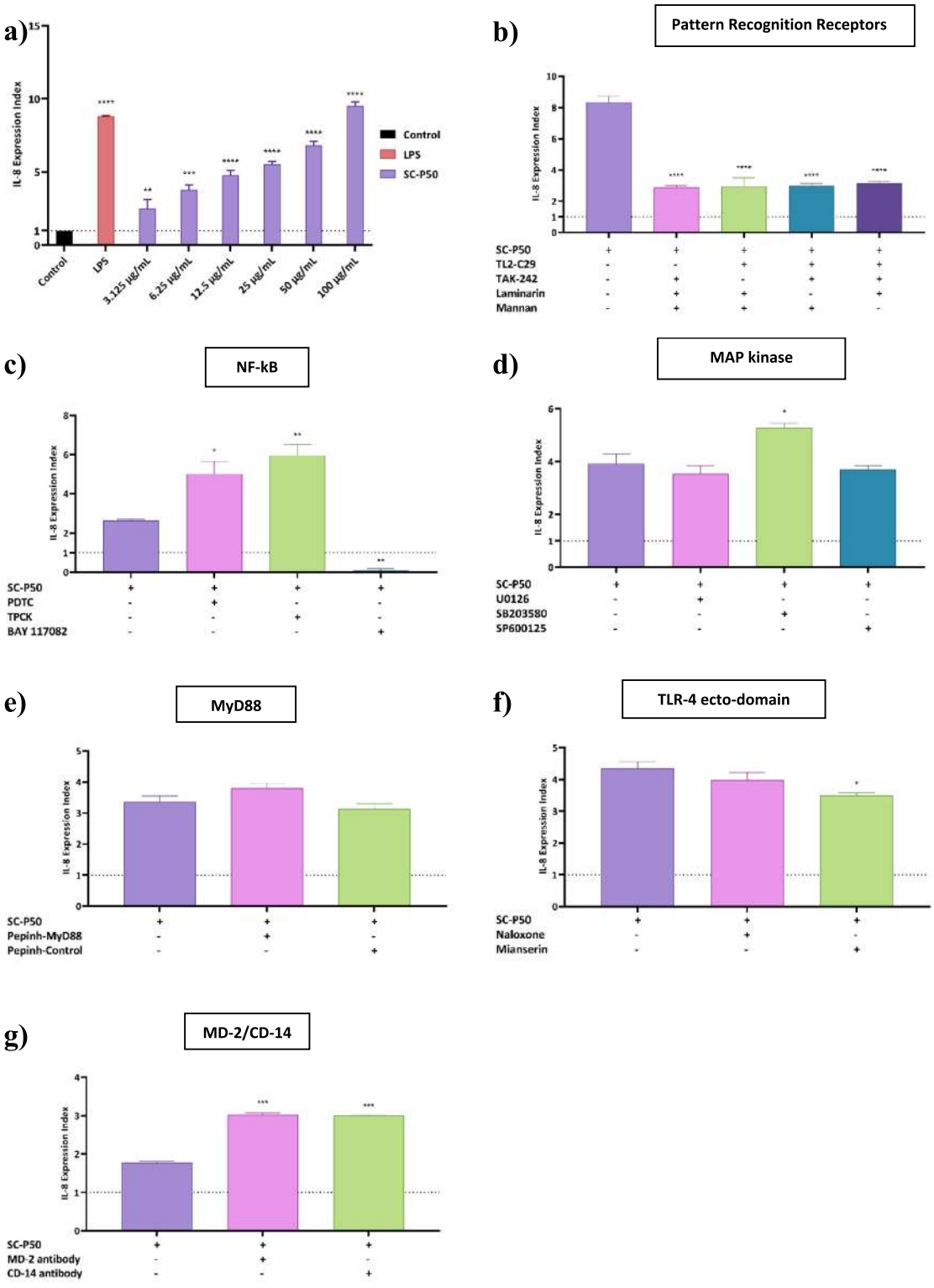

Fig. 11. Effect of pathway inhibitors on the upregulation of IL-8 expression by SC-P50 (100 μg/mL) with in IL-8 LucRep- RAW 264.7 cells. a). SC-P50 concentration-dependently increases the IL-8 expression index of IL-8 LucRep-RAW 264.7 cells. Positive control: LPS (1 μg/mL). Vehicle control: medium. (b-g) The IL-8 expression index of SC-P50 (100 μg/mL) was then measured the presence/absence of various inhibitors. b). utilised inhibitors of pattern recognition receptors (TLR2 (TL2-C29: 5 μg/mL); TLR4 (TAK-242: 5 μg/mL); Dectin-1 (laminarin: 300 μg/mL) and MR (mannan: 200 μg/mL). c). utilised NF-κB pathway inhibitors (PDTC: 300 μM; TPCK: 30 μM; BAY 117082: 30 μM). d). utilised MAPK pathway inhibitors (U0126: 10 μM; SB203580: 20 μM; SP600125: 20 μM). e). utilised MyD88 signalling pathway inhibitors (Pepinh-MyD88: 10 μM; Pepinh-MyD88: 10 μM). (F) utilised TLR4 ecto-domain inhibitors (Naloxone: 100 μM; Mianserin: 100 μM). g). utilised antibodies raised against TLR4 extracellular domain co-factors (MD-2 antibody: 5 μg/mL; CD-14 antibody: 10 μg/mL). *$P < 0.05$, **$P < 0.01$, *** $P < 0.001$ and ****$P < 0.0001$ compared with the respective control.

a)

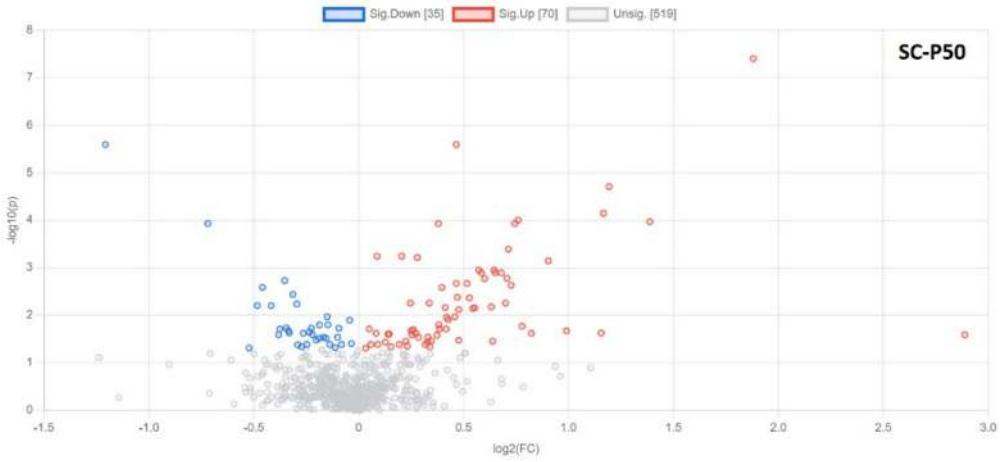

b)

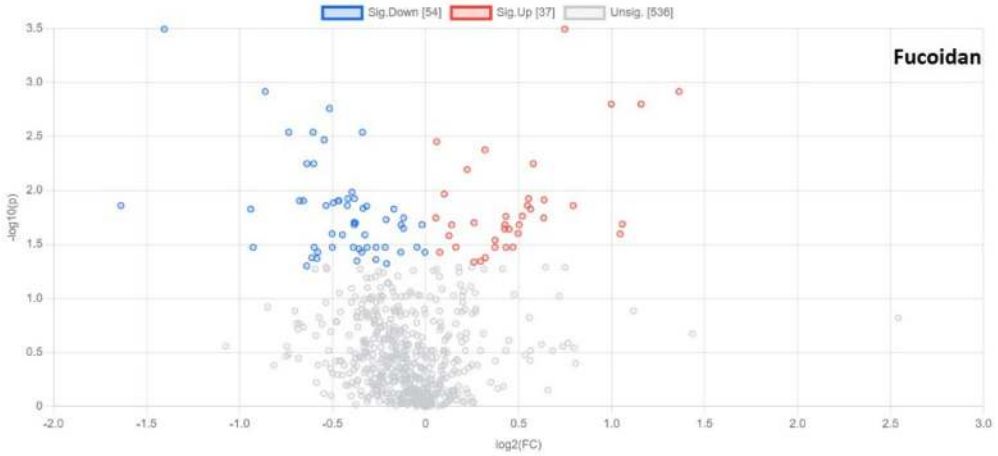

c)

METABOLITES COMMONLY ALTERED BY SC-P50 and FUCOIDAN

SIGNIFICANTLY INCREASED					SIGNIFICANTLY DECREASED		
C3-DC (C4-OH)	Cer(d16:1/24:0)	HexCer(d18:1/16:0)	PC aa C32:0	GCDCA	C2	DG(14:0_18:1)	p-Cresol-SO4
C4:1	Cer(d18:1/16:0)	HexCer(d18:1/23:0)	PC aa C36:1	PAG	C3	DG(14:0_18:2)	Spermine
CE(18:0)	Cer(d18:1/18:0)	HexCer(d18:1/24:0)	PC aa C40:1	Histamine	C5	DG(14:0_20:0)	t4-OH-Pro
	Cer(d18:1/23:0)	HexCer(d18:1/24:1)	PC aa C42:0	Cit		TG(16:1_34:2)	Thr
	Cer(d18:1/24:0)	HexCer(d18:1/26:0)	PC aa C42:1	HCys		TG(18:1_32:1)	1-Met-His
	Cer(d18:1/24:1)		PC aa C42:2				ADMA
	Cer(d18:2/16:0)		PC ae C34:0				Cys
	Cer(d18:2/22:0)		PC ae C36:0				Gly
	Cer(d18:2/24:0)		lysoPC a C24:0				
	Cer(d18:2/24:1)						
	DG(16:0_16:1)						
	DG(16:0_18:1)						

Fig. 12. Metabolic responses of RAW 264.7 cells to SC-P50 and fucoidan. Cells were exposed to various treatments for a period of 24 h, treatments were then removed, cells were gently washed and metabolites extracted by a published methodology (Andresen et al., 2022). Metabolites in extracts were quantified by LC-MS/MS using a commercially available kit, MxP Quant500 kit (Biocrates Life Science AG, Innsbruck, Austria). The concentrations of many intracellular metabolites were altered by exposure to a) SC-P50 or b) fucoidan at 1, 10 and 100 μg/mL. The plots indicate statistically significant (FDR < 0.05) metabolite changes. Those shaded in red were significantly increased (70 for SC-P50; 37 for fucoidan) and those in blue (35 for SC-P50; 54 for fucoidan) significantly decreased compared with culture medium (vehicle). c). Lists the metabolite levels commonly increased or decreased by both SC-50 and fucoidan.

responsible IL-8 secretion. SC-P50 must however, interact with other PPRs. For instance, the blockade of dectin-1 suppressed IL-8 secretion; and blockade of dectin-1, MR, TLR2 or TLR4 affects its IL-8 gene expression.

SC-P50 interacts with the TLR4 ectodomain, but intriguingly, does not involve the adaptor protein MyD88. SC-P50 could transduce TLR4 signalling through the TRIF pathway, but it is clear is that NF-κB signalling underlies NO production. Further probing of intracellular SC-P50 signalling is required to fully understand its mechanism of action, perhaps using gene knock-out or Western blotting methods that were not available during these studies.

The BioMAP analysis also enabled an unsupervised search for

mathematically similar profiles against a reference database of all previously tested compounds. SC-P50's profile closely aligned with that of fucoidan which shared 31 common activities. Fucoidan is a complex polysaccharide, occurring in species of brown seaweed (Li et al., 2008). It is structurally unrelated to SC-P50, being composed of repeating units of fucose along with other monosaccharides including galactose, xylose, and uronic acid (Anisha et al., 2022), but is extensively studied as a human health supplement. Fucoidan exhibits anti-inflammatory, antioxidant, antiviral, and anticancer properties by targeting various molecular components including enzymes, growth factors, and immune cells (Lin et al., 2020; Luthuli et al., 2019; Wijesekara et al., 2011; Zayed et al., 2024). Fucoidan was deemed a useful comparator compound, and when assayed stimulated concentration-dependent NO production comparable in potency to SC-P50 (Fig. S16a). It was not possible to conduct inhibitor studies for fucoidan, so it still must be determined whether SC-P50 and fucoidan share common receptors/signalling pathways, and that includes the TLR4-NF-κB pathway. The intracellular metabolomic profiles of macrophages, as determined by mass spectrometry, for SC-P50 and fucoidan treatment differed substantially from vehicle control; and although these responses were far from identical, there were many common metabolite changes. Ceramide and phosphotidylcholine increases, likely reflect cellular inflammatory responses and membrane remodelling. Common up- and down-regulation of acylcarnitines, reflect common effects on lipid metabolism. Both compounds affected metabolites mediating immunological responses, for example increased histamine and homocysteine and suppressed polyamines. Unique changes for SC-P50 were increased glutamine, lactate and ornithine levels. The metabolic changes in the macrophage cell, could indicate changes in the proportion M1 (pro-inflammatory) and M2 (anti-inflammatory/pro-resolving) phenotypes. Further studies should use flow cytometry to measure complex changes in immune cell populations as modulated by SC-P50 (Heieis et al., 2023; Jiang et al., 2022; Soto-Heredero et al., 2020; Viola et al., 2019). Although, it is notable that BioMAP profiling shows that SC-P50 is active in cells with either an M1-like or M2-like phenotype.

Finally, comparative studies with three commercially-available sources of sugar beet arabinan (Fig. S16b), showed that linear arabinan (only α-(1 → 5) *araf* linkages), a debranched arabinan (also only α-(1 → 5) *araf* linkages), and branched arabinan (α-(1 → 5) and α-(1 → 3) *araf* linkages) did not induce NO production. These had extremely weak effects of IL-8 secretion, even at 100 μg/mL (Fig. S16c). Arabinans are comprised of small amounts of monosaccharides other than *araf* (such as galactose, rhamnose and galacturonic acid) and differences in the amounts of these could explain differences in bioactivity. Another explanation is that α-(1 → 2) *araf* linkages in addition to α-(1 → 5), and α-(1 → 3) *araf* linkages (as found in SC-P50) are required for this bioactivity. The repeating pattern of α-(1 → 3) *araf*, α-(1 → 2) *araf* and α-(1 → 2)/(1 → 3) *araf* branching points are quite different to other natural sources (Wefers et al., 2018). Future studies should compare SC-P50 with a wider range of naturally occurring arabinans, especially where the polysaccharide structure is known. Structure-activity relationship (SAR) studies could then pinpoint the structural motifs involved in the bioactivities observed here.

There remains a pressing need to discover new immunomodulatory agents that can modulate adaptive immune responses. Enhancing the immune system's ability to fight bacterial infections could reduce the development of AMR, by circumventing bacteria's ability to become resistant to antimicrobial agents. The main limitations for SC-P50's further development are the lack of flow cytometry data (to understand SC-P50's effects on immune cell sub-types), and the lack of *in vivo* data (to demonstrate bioavailability and efficacy). *In vivo* studies using SC-P50 alone or in combination with other antimicrobial therapies appear to be a logical next step.

5. Conclusion

This investigation outlines the discovery and characterization of a unique arabinan occurring in the roots of *Sida cordifolia*. The unique structural features of this arabinan are its three motifs, the main one being an α-L-arabinofuranose disaccharide (A-(1 → 5)-D), where the A unit is completely substituted at *O*-2 and *O*-3 positions by α-L-arabinofuranose, while the minor motifs differ from the main one in the degree of substitution of the A unit, distinguishing it from other previously characterized arabinans. The immunomodulatory and metabolic activities of *Sida cordifolia* arabinan appear to be highly potent and act across a range of human cell types. Its actions appear focused on a select number of cytokines (IL-6, TNF-α, IL-8 and IL-2). The discovery of this novel polysaccharide provides a scientific basis for the known immunomodulatory properties of the *Sida cordifolia* plant and perhaps other plants of the mallow family. Very few polysaccharide immunomodulators have been characterized to the extent that SC-P50 has been here, and this could pave the way for *in vivo* studies in animals and humans.

CRediT authorship contribution statement

Fang Cheng: Writing – review & editing, Writing – original draft, Methodology, Investigation, Formal analysis, Data curation. **Xiaobei Pan:** Visualization, Methodology, Investigation, Formal analysis, Data curation, Conceptualization. **Anna Notaro:** Writing – review & editing, Visualization, Methodology, Investigation, Formal analysis, Data curation. **Andrea Iovine:** Visualization, Methodology, Investigation, Formal analysis, Data curation. **Antonio Molinaro:** Writing – review & editing, Visualization, Methodology, Investigation, Data curation. **Cristina De Castro:** Writing – review & editing, Visualization, Methodology, Investigation, Data curation. **Brian D. Green:** Writing – review & editing, Visualization, Supervision, Project administration, Methodology, Funding acquisition, Conceptualization.

Declaration of competing interest

BDG is a director and shareholder of Aramune Technologies Limited. All other authors declare that they have no conflicts of interest.

Acknowledgements

The studies that structurally elucidated polysaccharides were funded by a grant from the MRC Confidence in Concept (CiC) scheme (MC_PC_17175). Studies investigating the cellular activities of polysaccharides were funded by an EPSRC Impact Acceleration Account (IAA) Funding Award (EP/R511602/1). FC's PhD studies were co-funded by the China Scholarship Council (CSC No. 201906660016).

Appendix A. Supplementary data

Supplementary data to this article can be found online at https://doi.org/10.1016/j.carbpol.2025.123724.

Data availability

Data will be made available on request.

References

Andresen, C., Boch, T., Gegner, H. M., Mechtel, N., Narr, A., Birgin, E., … Hubschmann, D. (2022). Comparison of extraction methods for intracellular metabolomics of human tissues. *Frontiers in Molecular Biosciences, 9*, Article 932261. https://doi.org/10.3389/fmolb.2022.932261

Anisha, G. S., Padmakumari, S., Patel, A. K., Pandey, A., & Singhania, R. R. (2022). Fucoidan from marine macroalgae: Biological actions and applications in regenerative medicine, drug delivery systems and food industry. *Bioengineering (Basel), 9*(9). https://doi.org/10.3390/bioengineering9090472

Ayrapetyan, O. N., Obluchinskaya, E. D., Zhurishkina, E. V., Skorik, Y. A., Lebedev, D. V., Kulminskaya, A. A., & Lapina, I. M. (2021). Antibacterial properties of fucoidans from the brown algae Fucus vesiculosus L. of the Barents Sea. *Biology (Basel), 10*(1). https://doi.org/10.3390/biology10010067

Balducci, E., Papi, F., Capialbi, D. E., & Del Bino, L. (2023). Polysaccharides' structures and functions in biofilm architecture of antimicrobial-resistant (AMR) pathogens. *International Journal of Molecular Sciences, 24*(4). https://doi.org/10.3390/ijms24044030

Banchereau, J., Pascual, V., & O'Garra, A. (2012). From IL-2 to IL-37: The expanding spectrum of anti-inflammatory cytokines. *Nature Immunology, 13*(10), 925–931. https://doi.org/10.1038/ni.2406

Bickel, M. (1993). The role of interleukin-8 in inflammation and mechanisms of regulation. *Journal of Periodontology, 64*(5 Suppl), 456–460. https://www.ncbi.nlm.nih.gov/pubmed/8315568.

Biswas, S. K., & Mantovani, A. (2012). Orchestration of metabolism by macrophages. *Cell Metabolism, 15*(4), 432–437. https://doi.org/10.1016/j.cmet.2011.11.013

Chen, S., Saeed, A., Liu, Q., Jiang, Q., Xu, H., Xiao, G. G., … Duo, Y. (2023). Macrophages in immunoregulation and therapeutics. *Signal Transduction and Targeted Therapy, 8*(1), 207. https://doi.org/10.1038/s41392-023-01452-1

Costa, S. L., Silva, V. D., Dos Santos Souza, C., Santos, C. C., Paris, I., Munoz, P., & Segura-Aguilar, J. (2016). Impact of plant-derived flavonoids on neurodegenerative diseases. *Neurotoxicity Research, 30*(1), 41–52. https://doi.org/10.1007/s12640-016-9600-1

Dabravolski, S. A., Sukhorukov, V. N., Melnichenko, A. A., Khotina, V. A., & Orekhov, A. N. (2023). Potential application of the plant-derived essential oils for atherosclerosis treatment: Molecular mechanisms and therapeutic potential. *Molecules, 28*(15). https://doi.org/10.3390/molecules28155673

David, J. M., Dominguez, C., Hamilton, D. H., & Palena, C. (2016). The IL-8/IL-8R axis: A double agent in tumor immune resistance. *Vaccines (Basel), 4*(3). https://doi.org/10.3390/vaccines4030022

De Castro, C., Parrilli, M., Holst, O., & Molinaro, A. (2010). Chapter five - microbe-associated molecular patterns in innate immunity: Extraction and chemical analysis of gram-negative bacterial lipopolysaccharides. In M. Fukuda (Ed.), *480. Methods in enzymology* (pp. 89–115). Academic Press. https://doi.org/10.1016/S0076-6879(10)80005-9.

Dinda, B., Das, N., Dinda, S., Dinda, M., & SilSarma, I. (2015). The genus *Sida* L.–A traditional medicine: Its ethnopharmacological, phytochemical and pharmacological data for commercial exploitation in herbal drugs industry. *Journal of Ethnopharmacology, 176*, 135–176. https://doi.org/10.1016/j.jep.2015.10.027

Franco, C. I., Morais, L. C., Quintans-Junior, L. J., Almeida, R. N., & Antoniolli, A. R. (2005). CNS pharmacological effects of the hydroalcoholic extract of Sida cordifolia L. leaves. *Journal of Ethnopharmacology, 98*(3), 275–279. https://doi.org/10.1016/j.jep.2005.01.008

Franzotti, E. M., Santos, C. V., Rodrigues, H. M., Mourao, R. H., Andrade, M. R., & Antoniolli, A. R. (2000). Anti-inflammatory, analgesic activity and acute toxicity of Sida cordifolia L. (Malva-branca). *Journal of Ethnopharmacology, 72*(1–2), 273–277. https://doi.org/10.1016/s0378-8741(00)00205-1

Gonzalez Caldito, N. (2023). Role of tumor necrosis factor-alpha in the central nervous system: A focus on autoimmune disorders. *Frontiers in Immunology, 14*, Article 1213448. https://doi.org/10.3389/fimmu.2023.1213448

Gorshkova, T. A., Kozlova, L. V., & Mikshina, P. V. (2013). Spatial structure of plant cell wall polysaccharides and its functional significance. *Biochemistry (Moscow), 78*(7), 836–853. https://doi.org/10.1134/S0006297913070146

Guo, X., Yu, J., Wang, R., Peng, N., & Li, R. (2024). Deciphering the effect of phytosterols on Alzheimer's disease and Parkinson's disease: The mediating role of lipid profiles. *Alzheimer's Research & Therapy, 16*(1), 53. https://doi.org/10.1186/s13195-024-01424-9

Heieis, G. A., Patente, T. A., Almeida, L., Vrieling, F., Tak, T., Perona-Wright, G., … Everts, B. (2023). Metabolic heterogeneity of tissue-resident macrophages in homeostasis and during helminth infection. *Nature Communications, 14*(1), 5627. https://doi.org/10.1038/s41467-023-41353-z

Huang, H., Guo, F., Deng, X., Yan, M., Wang, D., Sun, Z., … Zhou, Q. (2022). Modulation of T cell responses by fucoidan to inhibit osteogenesis. *Frontiers in Immunology, 13*, Article 911390. https://doi.org/10.3389/fimmu.2022.911390

Huyke, C., Engel, K., Simon-Haarhaus, B., Quirin, K. W., & Schempp, C. M. (2007). Composition and biological activity of different extracts from Schisandra sphenanthera and Schisandra chinensis. *Planta Medica, 73*(10), 1116–1126. https://doi.org/10.1055/s-2007-981559

Iqbal, H., Wright, C. L., Jones, S., da Silva, G. R., McKillen, J., Gilmore, B. F., … Green, B. D. (2022). Extracts of Sida cordifolia contain polysaccharides possessing immunomodulatory activity and rosmarinic acid compounds with antibacterial activity. *BMC Complement Med Ther, 22*(1), 27. https://doi.org/10.1186/s12906-022-03502-7

Jang, D. I., Lee, A. H., Shin, H. Y., Song, H. R., Park, J. H., Kang, T. B., … Yang, S. H. (2021). The role of tumor necrosis factor alpha (TNF-alpha) in autoimmune disease and current TNF-alpha inhibitors in therapeutics. *International Journal of Molecular Sciences, 22*(5). https://doi.org/10.3390/ijms22052719

Jha, A. K., Huang, S. C., Sergushichev, A., Lampropoulou, V., Ivanova, Y., Loginicheva, E., … Artyomov, M. N. (2015). Network integration of parallel metabolic and transcriptional data reveals metabolic modules that regulate macrophage polarization. *Immunity, 42*(3), 419–430. https://doi.org/10.1016/j.immuni.2015.02.005

Jiang, Q., Qiu, Y., Kurland, I. J., Drlica, K., Subbian, S., Tyagi, S., & Shi, L. (2022). Glutamine is required for M1-like polarization of macrophages in response to Mycobacterium tuberculosis infection. *mBio, 13*(4), Article e0127422. https://doi.org/10.1128/mbio.01274-22

Jin, M., Zhao, K., Huang, Q., & Shang, P. (2014). Structural features and biological activities of the polysaccharides from Astragalus membranaceus. *International Journal of Biological Macromolecules, 64*, 257–266. https://doi.org/10.1016/j.ijbiomac.2013.12.002

Kaur, S., Bansal, Y., Kumar, R., & Bansal, G. (2020). A panoramic review of IL-6: Structure, pathophysiological roles and inhibitors. *Bioorganic & Medicinal Chemistry, 28*(5), Article 115327. https://doi.org/10.1016/j.bmc.2020.115327

Khairy, A., Ghareeb, D. A., Celik, I., Hammoda, H. M., Zaatout, H. H., & Ibrahim, R. S. (2023). Forecasting of potential anti-inflammatory targets of some immunomodulatory plants and their constituents using in vitro, molecular docking and network pharmacology-based analysis. *Scientific Reports, 13*(1), 9539. https://doi.org/10.1038/s41598-023-36540-3

Klos, P., & Chlubek, D. (2022). Plant-derived terpenoids: A promising tool in the fight against melanoma. *Cancers (Basel), 14*(3). https://doi.org/10.3390/cancers14030502

Koizumi, K. (2002). Chapter 3 HPLC of carbohydrates on graphitized carbon columns. In Z. E. Rassi (Ed.), *Vol. 66. Journal of Chromatography Library* (pp. 103–119). Elsevier. https://doi.org/10.1016/S0301-4770(02)80028-8.

Kotake, T., Yamanashi, Y., Imaizumi, C., & Tsumuraya, Y. (2016). Metabolism of L-arabinose in plants. *Journal of Plant Research, 129*(5), 781–792. https://doi.org/10.1007/s10265-016-0834-z

Lai, X., Chow, S. H., Le Brun, A. P., Muir, B. W., Bergen, P. J., White, J., … Shen, H.-H. (2024). Polysaccharide-targeting lipid nanoparticles to kill Gram-negative bacteria. *Small, 20*(6), Article 2305052. https://doi.org/10.1002/smll.202305052

Laskin, D. L. (2009). Macrophages and inflammatory mediators in chemical toxicity: A battle of forces. *Chemical Research in Toxicology, 22*(8), 1376–1385. https://doi.org/10.1021/tx900086v

Leonard, E. K., Tomala, J., Gould, J. R., Leff, M. I., Lin, J. X., Li, P., … Spangler, J. B. (2024). Engineered cytokine/antibody fusion proteins improve IL-2 delivery to pro-inflammatory cells and promote antitumor activity. *JCI Insight, 9*(18), Article e173469. https://doi.org/10.1172/jci.insight.173469

Li, B., Lu, F., Wei, X., & Zhao, R. (2008). Fucoidan: Structure and bioactivity. *Molecules, 13*(8), 1671–1695. https://doi.org/10.3390/molecules13081671

Lin, Z., Tan, X., Zhang, Y., Li, F., Luo, P., & Liu, H. (2020). Molecular targets and related biologic activities of fucoidan: A review. *Marine Drugs, 18*(8). https://doi.org/10.3390/md18080376

Luthuli, S., Wu, S., Cheng, Y., Zheng, X., Wu, M., & Tong, H. (2019). Therapeutic effects of fucoidan: A review on recent studies. *Marine Drugs, 17*(9). https://doi.org/10.3390/md17090487

Michalak, M. (2022). Plant-derived antioxidants: Significance in skin health and the ageing process. *International Journal of Molecular Sciences, 23*(2). https://doi.org/10.3390/ijms23020585

Murphy, E. J., Fehrenbach, G. W., Abidin, I. Z., Buckley, C., Montgomery, T., Pogue, R., … Rezoagli, E. (2023). Polysaccharides-naturally occurring immune modulators. *Polymers (Basel), 15*(10). https://doi.org/10.3390/polym15102373

Panggabean, J. A., Adiguna, S. P., Rahmawati, S. I., Ahmadi, P., Zainuddin, E. N., Bayu, A., & Putra, M. Y. (2022). Antiviral activities of algal-based sulfated polysaccharides. *Molecules, 27*(4), Article 1178. https://doi.org/10.3390/molecules27041178

Peng, J., Zheng, T. T., Li, X., Liang, Y., Wang, L. J., Huang, Y. C., & Xiao, H. T. (2019). Plant-derived alkaloids: The promising disease-modifying agents for inflammatory bowel disease. *Frontiers in Pharmacology, 10*, 351. https://doi.org/10.3389/fphar.2019.00351

Pillai, M. G., & Antony, H. (2024). Harnessing the immunomodulatory potential of natural products in precision medicine: A comprehensive review. *Exploration of Drug Science, 2*(3), 339–360. https://doi.org/10.37349/eds.2024.00050

Qazi, B. S., Tang, K., & Qazi, A. (2011). Recent advances in underlying pathologies provide insight into interleukin-8 expression-mediated inflammation and angiogenesis. *Int J Inflam, 2011*, Article 908468. https://doi.org/10.4061/2011/908468

Rajasekaran, S., Rajasekar, N., & Sivanantham, A. (2021). Therapeutic potential of plant-derived tannins in non-malignant respiratory diseases. *The Journal of Nutritional Biochemistry, 94*, Article 108632. https://doi.org/10.1016/j.jnutbio.2021.108632

Rodrigues, F. C., & de Oliveira, A. F. M. (2020). The genus Sida L. (Malvaceae): An update of its ethnomedicinal use, pharmacology and phytochemistry. *South African Journal of Botany, 132*, 432–462. https://doi.org/10.1016/j.sajb.2020.04.030

Samtiya, M., Aluko, R. E., Dhewa, T., & Moreno-Rojas, J. M. (2021). Potential health benefits of plant food-derived bioactive components: An overview. *Foods, 10*(4). https://doi.org/10.3390/foods10040839

Sharma, R., Fu, S. M., & Ju, S. T. (2011). IL-2: A two-faced master regulator of autoimmunity. *Journal of Autoimmunity, 36*(2), 91–97. https://doi.org/10.1016/j.jaut.2011.01.001

Shen, Y., Zhao, H., Wang, X., Wu, S., Wang, Y., Wang, C., … Zhao, H. (2024). Unraveling the web of defense: The crucial role of polysaccharides in immunity. *Frontiers in Immunology, 15*, Article 1406213. https://doi.org/10.3389/fimmu.2024.1406213

Sindhu, R. K., Goyal, A., Das, J., Neha, Choden, S., & Kumar, P. (2021). Immunomodulatory potential of polysaccharides derived from plants and microbes: A narrative review. *Carbohydrate Polymer Technologies and Applications, 2*, Article 100044. https://doi.org/10.1016/j.carpta.2021.100044

Song, S., Peng, H., Wang, Q., Liu, Z., Dong, X., Wen, C., … Zhu, B. (2020). Inhibitory activities of marine sulfated polysaccharides against SARS-CoV-2. *Food & Function, 11*(9), 7415–7420. https://doi.org/10.1039/d0fo02017f

Soto-Heredero, G., de Las, G., Heras, M. M., Gabande-Rodriguez, E., Oller, J., & Mittelbrunn, M. (2020). Glycolysis - a key player in the inflammatory response. *The FEBS Journal, 287*(16), 3350–3369. https://doi.org/10.1111/febs.15327

Speciale, I., Notaro, A., Garcia-Vello, P., Di Lorenzo, F., Armiento, S., Molinaro, A., … De Castro, C. (2022). Liquid-state NMR spectroscopy for complex carbohydrate structural analysis: A hitchhiker's guide. *Carbohydrate Polymers, 277*, Article 118885. https://doi.org/10.1016/j.carbpol.2021.118885

Surayot, U., & You, S. (2017). Structural effects of sulfated polysaccharides from Codium fragile on NK cell activation and cytotoxicity. *International Journal of Biological Macromolecules, 98*, 117–124. https://doi.org/10.1016/j.ijbiomac.2017.01.108

Tabarsa, M., You, S., Yelithao, K., Palanisamy, S., Prabhu, N. M., & Nan, M. (2020). Isolation, structural elucidation and immuno-stimulatory properties of polysaccharides from Cuminum cyminum. *Carbohydrate Polymers, 230*, Article 115636. https://doi.org/10.1016/j.carbpol.2019.115636

Tanaka, T., Narazaki, M., & Kishimoto, T. (2014). IL-6 in inflammation, immunity, and disease. *Cold Spring Harbor Perspectives in Biology, 6*(10), Article a016295. https://doi.org/10.1101/cshperspect.a016295

Tokunaga, R., Zhang, W., Naseem, M., Puccini, A., Berger, M. D., Soni, S., … Lenz, H. J. (2018). CXCL9, CXCL10, CXCL11/CXCR3 axis for immune activation - a target for novel cancer therapy. *Cancer Treatment Reviews, 63*, 40–47. https://doi.org/10.1016/j.ctrv.2017.11.007

Vats, D., Mukundan, L., Odegaard, J. I., Zhang, L., Smith, K. L., Morel, C. R., … Chawla, A. (2006). Oxidative metabolism and PGC-1beta attenuate macrophage-mediated inflammation. *Cell Metabolism, 4*(1), 13–24. https://doi.org/10.1016/j.cmet.2006.05.011

Viola, A., Munari, F., Sanchez-Rodriguez, R., Scolaro, T., & Castegna, A. (2019). The metabolic signature of macrophage responses. *Frontiers in Immunology, 10*, 1462. https://doi.org/10.3389/fimmu.2019.01462

Wefers, D., Florchinger, R., & Bunzel, M. (2018). Detailed structural characterization of arabinans and galactans of 14 apple cultivars before and after cold storage. *Frontiers in Plant Science, 9*, 1451. https://doi.org/10.3389/fpls.2018.01451

Wijesekara, I., Pangestuti, R., & Kim, S.-K. (2011). Biological activities and potential health benefits of sulfated polysaccharides derived from marine algae. *Carbohydrate Polymers, 84*(1), 14–21. https://doi.org/10.1016/j.carbpol.2010.10.062

Xue, S., Zhou, Y., Zhang, J., Xiang, Z., Liu, Y., Miao, T., Liu, G., Liu, B., Liu, X., & Shen, L. (2019). Anemoside B4 exerts anti-cancer effect by inducing apoptosis and autophagy through inhibition of PI3K/Akt/mTOR pathway in hepatocellular carcinoma. *American Journal of Translational Research, 11*(4).

Zayed, A., Al-Saedi, D. A., Mensah, E. O., Kanwugu, O. N., Adadi, P., & Ulber, R. (2024). Fucoidan's molecular targets: A comprehensive review of its unique and multiple targets accounting for promising bioactivities supported by in silico studies. *Marine Drugs, 22*(1), 29. https://doi.org/10.3390/md22010029

Zebeaman, M., Tadesse, M. G., Bachheti, R. K., Bachheti, A., Gebeyhu, R., & Chaubey, K. K. (2023). Plants and plant-derived molecules as natural immunomodulators. *BioMed Research International, 2023*, Article 7711297. https://doi.org/10.1155/2023/7711297